Markus Richter, BSc

Phase diagram of the extended Hubbard model including spin-orbit coupling on a honeycomb lattice

MASTER'S THESIS

to achieve the university degree of

Diplom-Ingenieur

Master's degree programme: Technical Physics

submitted to

Graz University of Technology

Supervisor

Assoc.Prof. Dipl.-Ing. Dr.techn. Markus Aichhorn

Institute of Theoretical and Computational Physics

Graz, August 2018

AFFIDAVIT

I declare that I have authored this thesis independently, that I have not used other than the declared sources/resources, and that I have explicitly indicated all material which has been quoted either literally or by content from the sources used. The text document uploaded to TUGRAZonline is identical to the present master's thesis.

_____   _____
            Date   Signature

Abstract

In 2004, by isolating single layers of graphite, the 2D-Material Graphene was found, giving rise to a huge amount of research papers investigating on its fascinating electronic, magneto-electronic and opto-electronic properties. One year later, the existence of a quantum spin Hall state was proposed for lattices of the honeycomb type, as realized in graphene, by including spin-orbit coupling. This was the starting point for the completely new field of topological insulators. In this thesis we use the honeycomb lattice as a playground to investigate the effects of strong correlations, non-local interactions, and spin-orbit coupling, using one orbital per site at half filling. The model Hamiltonian of our choice is the extended Hubbard model with an additional spin-orbit coupling term. This model provides, besides the unordered phase, two ordered phases, namely spin density waves (SDW) and charge density waves (CDW), as well as the additional characterization of being topologically trivial or non-trivial.

To analyze the interplay between the different phases we calculated phase diagrams using mean-field theory (MFT), and further compared them to calculations performed with the more sophisticated method of dynamic mean field theory (DMFT).

Kurzfassung

Im Jahr 2004 wurde durch Isolierung einzelner Graphitschichten das 2D-Material Graphen entdeckt was einer großen Anzahl von Forschungsarbeiten zur Folge hatte, die sich damit beschäftigten die elektronischen, magneto-elektronischen und opto-elektronischen Eigenschaften zu untersuchen.

Im darauffolgenden Jahr wurde die Existenz eines Quanten-Spin-Hall-Zustandes für das Bienenwabengitter, wie es in Graphen realisiert ist, durch Einbeziehung der Spin-Bahn-Kopplung vorgeschlagen. Dies war der Ausgangspunkt für das völlig neue Gebiet der topologischen Isolatoren. In dieser Arbeit verwenden wir das Bienenwabengitter, um die Auswirkungen von starken Korrelationen, nicht-lokalen Wechselwirkungen und Spin-Bahn-Kopplung zu untersuchen. Hierfür verwenden wir das erweiterte Hubbard-Modell mit einem Orbital pro Gitterplatz bei halber Füllung und ergänzen selbiges um einen zusätzlichem Spin-Orbit Kopplungsterm. Dieses Modell liefert neben der ungeordneten Phase, zwei geordnete Phasen, bekannt als Spindichtewellen (SDW) und Ladungsdichtewellen (CDW). Zusätzlich erhalten wir eine weitere Charakterisierung in topologisch trivial oder nicht-trivial. Um das Zusammenspiel der verschiedenen Phasen zu analysieren, haben wir zunächst unter Verwendung der Mean-Field-Theorie (MFT) Phasendiagramme berechnet und dann die Ergebnisse mit weiteren Berechnungen unter Zuhilfenahme der ausgefeilteren dynamischen Mean-Field-Theorie (DMFT) verglichen.

Acknowledgments

I own my gratitude to Prof. Markus Aichhorn, for the supervision of my thesis and for giving me the opportunity to work on this interesting topic. He has always been supportive and I am truly thankful for the remarkable clarity he is able to answer any kind of question.

I especially want to thank Robert Triebl for his interest in my work. He never became tired of answering all my larger and minor questions and helped me fixing many issues. Without him and his previous work, my thesis would not have been possible.

I am thankful to Gernot Kraberger for his willingness to share all his knowledge about DMFT and to Hermann Schnait for all the fruitful conversations we had.

I truly enjoyed working at the Institute of Theoretical and Computational Physics, and want to thank all its members for providing a good working atmosphere at the office. The discussions during lunch-time - not just about physics, made working here a real pleasure.

I am very grateful to the TRIQS-team for providing such a useful and compact tool to perform DMFT calculations (and more), and making it available to everyone.

Last, but not least I want to thank my friends and family, for their ever lasting support and encouragement. Especially thanks to my parents for their financial support and unconditional reassurance and most importantly to Carina, for her love, understanding and relentless patience throughout this whole time.

Contents

Introduction

When in 1946 Philip Russel Wallace theoretically first described the electronic properties of Graphene [1], not even he himself did believe that such a two dimensional material could exist in nature. In fact, he used it as an approximation for the three-dimensional Graphite. However, in 2004 Geim and Novoselov [2] managed to isolate these single layers of the carbon crystal for the first time, and exceptional interest for this exotic material was born among theorists as well as experimentalists. They found a material that has many desirable properties united. Due to its structure and the low atomic number of carbon it obviously is thin and light. Additionally, the crystal provides more not so intuitive characteristics. Its unique band structure lets electrons, that travel through the lattice, behave similar to light and hence gives rise to extraordinarily good conductivity. Besides, the arrangement of carbon atoms on the honeycomb lattice makes it one of the strongest materials ever found.

The honeycomb lattice itself gave rise to a completely new type of materials. In 2005 Kane and Mele proposed the existence of a quantum spin Hall effect (QSHE) [3, 4], which compares to the similar quantum Hall effect but does not require a strong external magnetic field. Differently, the effect is caused by strong spin-orbit coupling. The generalization of this QSHE to other dimensions is what we refer today to as topological insulators, which are materials that are insulating in the bulk and conducting on the edges of the sample. These edge states are especially interesting as they are also insensitive to disorders and interactions.

Apart from that, the topic of strongly-correlated systems has come more and more into the focus of today's condensed matter physics, as they often show unusual electronic and magnetic properties. The standard model Hamiltonian to investigate on such systems is the so called Hubbard model, which consist of a tight-binding term and an on-site interaction term. Nonetheless, studies have shown that in case of dimensional constraint also non-local interactions need to be considered making it reasonable to in-

clude further terms to the Hamiltonian. The natural expansion of the Hubbard model is the extended Hubbard model, where nearest-neighbor interactions are additionally considered.

The aim of this thesis is to investigate on the different phases and transitions between them, using an extended Hubbard model with additional spin-orbit coupling on a honeycomb lattice. For this purpose it is split into two parts: the non-relativistic treatment consisting just of the extended Hubbard model and the relativistic treatment including spin-orbit coupling.

In the first chapter we provide the theoretical background to the (extended) Hubbard model and discuss the appearance of the different phases namely spin density waves (SDW), charge density waves (CDW) and an unordered phase caused by the dominance of one parameter respective to the others. Further, two methods in order to calculate the phase diagram for the extended Hubbard model are explained and the according results are shown. Therefore, we start with mean-field theory (MFT) as a very simple approximation obtained by neglecting spatial fluctuations to get a qualitative idea. Afterwards, local quantum fluctuations are recovered by the application of the more accurate approximation of dynamic mean-field theory (DMFT).

Finally in the second chapter a brief overview on the field of topological insulators is given and thereafter spin-orbit coupling is added to the model to study the interplay between spin-orbit coupling and strong correlations. Besides, the consequence of the broken degeneracy of the spin-orientations is discussed and for MFT the two possibilities of out-of and in-plane magnetization are calculated. In DMFT we consider just the easier, but energetically non-favorable out-of plane magnetization.

Chapter 1

Non-relativistic treatment

The full Hamiltonian that describes any molecule or solid (in a non-relativistic manner), given in atomic units, reads

$$\hat{H} = -\frac{1}{2}\sum_i \nabla_i^2 - \sum_\alpha \frac{1}{2M_\alpha}\nabla_\alpha^2 - \sum_{\alpha,i}\frac{Z_\alpha}{|\mathbf{r}_i - \mathbf{R}_\alpha|} + \sum_{i<j}\frac{1}{|\mathbf{r}_i - \mathbf{r}_j|} + \sum_{\alpha<\beta}\frac{Z_\alpha Z_\beta}{|\mathbf{R}_\alpha - \mathbf{R}_\beta|} \quad (1.1)$$

where α and β are nuclei indices and i and j electron indices of the system, $\mathbf{R}_\alpha$ and $\mathbf{r}_i$ are the positions of the nuclei and electrons, M_α and Z_α labels the mass and charge of the nuclei.

The first two terms describe the kinetic energy and the last three terms the potential energy of all particles in the system. The third term is caused by the attractive coulomb force between every electron and every nucleus, and the last two terms by the repulsive intra-nucleus and intra-electron Coulomb force.

Even though it is simple to write down this Hamiltonian, it is for almost every system impossible to be solved.

Solving means finding the eigenstates E_ν and eigenenergies $|\Psi_\nu\rangle$ of the Hamiltonian (1.1)

$$\hat{H}|\Psi_\nu\rangle = E_\nu|\Psi_\nu\rangle. \quad (1.2)$$

The only exact solution can be found for the hydrogen atom, as this consists only of one proton and one electron.

As a first simplification usually the Born-Oppenheimer approximation is applied, which takes into account that due to the much bigger mass of the nuclei compared to the electrons (more than 10^3 times larger), the nuclei move a lot slower and can therefore

be fixed in position to calculate the energy. This makes the second term in eq. (1.1) vanish and the last term become a constant. As a constant in the Hamiltonoperator just gives an overall energy-shift which can always be subtracted or added at any point, one is left with the remaining three terms

$$
\hat{H} = \underbrace{\frac{1}{2} \sum_i \nabla_i^2}_{\text{kinetic energy}} - \underbrace{\sum_{\alpha,i} \frac{Z_\alpha}{|\mathbf{r}_i - \mathbf{R}_\alpha|}}_{\text{lattice potential}} + \underbrace{\sum_{i<j} \frac{1}{|\mathbf{r}_i - \mathbf{r}_j|}}_{\text{interaction}} \tag{1.3}
$$

Still, this problem turns out to need further simplifications in order to be solved. The reason is the electron-electron interaction, that leaves it still a complex many-body problem.

The easiest approximation can be found by simply neglecting the interaction-part. However this so-called free-electron approximation is just suitable for metals, where electrons are delocalized over the whole crystal, and it catastrophically fails for semiconductors or insulators. But even more sophisticated models like the density functional theory (DFT), whereby the electron-electron interaction is included via an effective potential are not satisfactory in the description of strongly-correlated materials.

In the following chapters we will go over to second-quantization, which is a more convenient description to deal with many-body problems and eventually introduce the (extended) Hubbard model.

1.1 Second quantization

When we go over from a one-particle to a many-particle description we could naively write down the many-body state as a product of one-particle states

$$
\left| \phi^N \right\rangle = \left| \phi_1^{(1)} \right\rangle \left| \phi_2^{(2)} \right\rangle \ldots \left| \phi_N^{(N)} \right\rangle = \left| \phi_1^{(1)}, \phi_2^{(2)} \ldots \phi_N^{(N)} \right\rangle = \prod_{i=1}^N \left| \phi_i^{(i)} \right\rangle \tag{1.4}
$$

where N gives the total number of particles, the superscript is the particle number and the subscript labels the state index. But identifying a particle with a state, requires them to be distinguishable.

Identical particles hold the same properties like spin, mass, volume, charge, magnetic momentum, etc. Since identical particles are indistinguishable any observable must stay the same under the permutation of two or more particles.

For electrons (fermions) this means that a correct description has the form of a totally

antisymmetric wave function $\left|\phi^N\right\rangle_{(-)}$, which can be written in the form of a so-called Slater-determinant:

$$\left|\phi^N\right\rangle_{(-)} = \hat{S}_- \prod_{i=1}^{N}\left|\phi_i^{(i)}\right\rangle = \frac{1}{N!}\begin{vmatrix} \left|\phi_1^{(1)}\right\rangle & \left|\phi_1^{(2)}\right\rangle & \cdots & \left|\phi_1^{(N)}\right\rangle \\ \left|\phi_2^{(1)}\right\rangle & \left|\phi_2^{(2)}\right\rangle & \cdots & \left|\phi_2^{(N)}\right\rangle \\ \vdots & \vdots & \ddots & \vdots \\ \left|\phi_N^{(1)}\right\rangle & \left|\phi_N^{(2)}\right\rangle & \cdots & \left|\phi_N^{(N)}\right\rangle \end{vmatrix}, \tag{1.5}$$

where $\hat{S}_-$ is the anti-symmetrization operator and $\frac{1}{N!}$ the normalization factor. Exchanging two columns (this is equal to the permutation of two particles) changes the determinant's sign, as it is required for anti-symmetry. Besides, as the determinant always vanishes when two rows or columns are equal, no two electrons are allowed to occupy the same state (this fulfills the Pauli principle).

1.1.1 Occupation number representation

As equation (1.5) is a rather complicated description of (fermionic) many-body states one therefore chooses the more convenient occupation-number description, which does not require to label indistinguishable particles

$$\left|\phi^N\right\rangle_{(-)} = \left|n_1, n_2, \ldots\right\rangle \tag{1.6}$$

with

$$\sum_i n_i = N, \tag{1.7}$$

where n_i is the number of particles in state i, that for fermions must either be zero or one (Pauli principle). To change particle numbers, creation $c_i^\dagger$ and annihilation c_i operators are used

$$\begin{aligned} c_i^\dagger \left|n_1 \ldots n_i \ldots\right\rangle &= \sqrt{n_i+1}\left|n_1 \ldots (n_i+1)\ldots\right\rangle \\ c_i \left|n_1 \ldots n_i \ldots\right\rangle &= \sqrt{n_i}\left|n_1 \ldots (n_i-1)\ldots\right\rangle \end{aligned} \tag{1.8}$$

Repeatedly applying the creation operator onto the vacuum state $\left|0\right\rangle$ gives the occupation number representation

$$\left|(n_1=1)\ldots(n_i=1),(n_j=1)\ldots\right\rangle = c_1^\dagger \ldots c_i^\dagger c_j^\dagger \ldots \left|0\right\rangle. \tag{1.9}$$

The anti-symmetrization of the state is encoded in the anti-commutation relations of the creation and annihilation operators

$$
\begin{aligned}
\{c_i, c_j^\dagger\} &= c_i c_j^\dagger + c_j^\dagger c_i = \delta_{ij} \\
\{c_i, c_j\} &= \{c_i^\dagger, c_j^\dagger\} = 0
\end{aligned}
\tag{1.10}
$$

$$
\Rightarrow c_i^\dagger c_j^\dagger = -c_j^\dagger c_i^\dagger.
\tag{1.11}
$$

This means that equation (1.9) is already a correctly anti-symmetrized representation of a fermionic many-body state. Equation (1.11) must be zero on both sides in the case $i = j$ which guarantees that the occupation number of one state cannot exceed one.

1.1.2 Operators in second quantization

To find a representation of observables in second quantization the corresponding operators need to be expressed in terms of creation and annihilation operators.
The simplest example is given by the number operator

$$
\hat{n}_i^c = c_i^\dagger c_i,
\tag{1.12}
$$

counting the occupation number of a given state i.

A general operator in every physical relevant case can be written as a sum of one-particle and two-particle operators, i.e., the individual terms depend and act only on one or two particle coordinates.
One-particle operators have the generic form

$$
\hat{T} = \sum_\alpha \hat{t}_{(\alpha)},
\tag{1.13}
$$

where $\hat{t}_{(\alpha)}$ can for instance be the kinetic energy or a external potential. In second quantization this becomes (for $\hat{t}_\alpha$ being the kinetic energy $\frac{1}{2}\nabla^2_{(\alpha)}$)

$$
\begin{aligned}
\hat{T} &= \sum_{ij} t_{ij} c_i^\dagger c_j \\
t_{ij} &= \int d\mathbf{r}\, \phi_i^*(\mathbf{r}) \frac{1}{2}\nabla^2_{(\alpha)} \phi_j(\mathbf{r'}),
\end{aligned}
\tag{1.14}
$$

with the transition matrix-element t_{ij} giving the transition from one orbital $|\phi_i\rangle$ to another $|\phi_j\rangle$. Hereby it should be stressed that $\phi_i^*(\mathbf{r})$ are Wannier functions (see appendix A), which are, similar to molecular orbitals, localized around the individual lattice sites in the crystal.

Similarly the two-particle operator

$$\hat{F} = \frac{1}{2} \sum_{\alpha \neq \beta} \hat{f}_{(\alpha,\beta)} \tag{1.15}$$

can be expressed in second quantization as follows

$$\hat{F} = \frac{1}{2} \sum_{ijkm} f_{ijkm} c_i^\dagger c_j^\dagger c_m c_k$$

$$f_{ijkm} = \int d\mathbf{r} d\mathbf{r}' \phi_i^*(\mathbf{r}) \phi_j^*(\mathbf{r}') V(|\mathbf{r} - \mathbf{r}'|) \phi_k(\mathbf{r}) \phi_m(\mathbf{r}') \tag{1.16}$$

1.2   The Hubbard model

A very successful model to describe solids in which electron correlations cannot be neglected is the Hubbard model, where electrons are rather confined to the atoms, but can tunnel from one atom to the nearest neighboring one. So one can talk about electrons sitting on one specific atom (or lattice site) or hop from one atom to a neighboring atom. Further, electron-electron interactions are just considered for two electrons sitting on the same site. For the elementary situation of one orbital per site this is equivalent to setting the f_{ijkm} in (1.16) equal to zero except for the case of coinciding indices, namely

$$f_{ijkm} = \begin{cases} U & \text{for } i = j = k = m \\ 0 & \text{else} \end{cases} \tag{1.17}$$

Together with the definition of the number operator (equation (1.12)), the Hubbard model thus reads

$$H = -\sum_{\langle ij \rangle, \sigma} t_{ij} c_{i\sigma}^\dagger c_{j\sigma} + U \sum_i n_{i\uparrow}^c n_{i\downarrow}^c + \epsilon_0 \sum_{i\sigma} n_{i\sigma}^c. \tag{1.18}$$

The hopping energy t_{ij} is given by the overlap between two neighboring atomic orbitals and U is the repulsive Coulomb potential of two electrons within the same orbital.

The third term, which describes the orbital energy, could in a single orbital system be removed as this again just gives a constant shift to the energy. Summing over $\langle ij \rangle$ means, that just nearest neighbors are taken into account and σ labels the spin (up $\uparrow$ and down $\downarrow$).

$n_{i\uparrow}^c n_{i\downarrow}^c$ gives the only remaining term $(n_{i\uparrow}^c n_{i\downarrow}^c = n_{i\downarrow}^c n_{i\uparrow}^c)$ of the on-site interaction which does not vanish due to the anti-commutation rules of equation (1.10). In the absence of hopping, there are 4 eigenstates for the atom $(|0\rangle, |\uparrow\rangle, |\downarrow\rangle, |\uparrow\downarrow\rangle)$ with the eigenenergies: $(0, \epsilon_0, \epsilon_0, U + 2\epsilon_0)$

1.2.1 Screening and the extended Hubbard model

The reason why reducing the electron-electron interaction to an on-site phenomenon is a quite good assumption for many 3D materials is the 'screening effect'.

Other than the Coulomb potential of a free charge, that decreases with the distance r proportional to $\frac{1}{r}$, a charge surrounded by movable charge-carriers is screened, i.e., the electric field is reduced exponentially

$$\frac{Z}{r} \underset{\text{screening}}{\rightarrow} \frac{Z}{r} e^{-r/\lambda} \tag{1.19}$$

where Z gives the charge number and λ a characteristic screening length. In a 3D-material the length will typically be short enough that just electrons sitting on the same atom 'feel' each other, and considering just on-site interactions will be a good approximation.

On the other hand, for two dimensional materials this assumption does not hold anymore. Due to the reduced density of electrons, caused by the lower dimension, the screening effect becomes weaker and further non-local interactions need to be taken into account. This brings us to the definition of the extended Hubbard model

$$H = -t \sum_{\langle ij \rangle, \sigma} c_{i\sigma}^\dagger c_{i\sigma} + U \sum_i n_{i\uparrow}^c n_{i\downarrow}^c + W \sum_{\langle ij \rangle} n_i^c n_j^c \tag{1.20}$$

with

$$n_i^c = n_{i\uparrow}^c + n_{i\downarrow}^c \tag{1.21}$$

where W now gives the strength of electron-electron interaction between the electrons of neighboring atoms. Here the term for the on-site energy has been removed (as in our

case it just gives a constant).

To get a qualitative picture of what happens in the cases that one parameter is dominant against the other two parameters, we look at the case of an infinite one dimensional atomic string at half filling. We find for a vanishing nearest neighbor and a large on-site interaction that an electron hopping away from the ground-state configuration (energy 0) gets penalized by an energy of U. Similarly, the inverted situation ($U = 0, W/t \ll$) leads to an energy-penalty of 3 W. In the final case that t is the dominant parameter the act of hopping is energetically favorable and the totally unordered system will be preferred, which is equivalent to the delocalization of electrons in metals. The situation is documented in table 1.1

case	configuration	energy	preferred ordering
$W = 0, \frac{U}{t} \gg 1$	$\cdots \uparrow\circ \ \downarrow\circ \ \uparrow\circ \ \downarrow\circ \ \cdots$	0	SDW
	$\cdots \uparrow\circ \ \ \circ \ \uparrow\downarrow\circ \ \downarrow\circ \ \cdots$	U	
$U = 0, \frac{W}{t} \gg 1$	$\cdots\uparrow\downarrow\circ \ \ \circ \ \uparrow\downarrow\circ \ \ \circ \ \cdots$	0	CDW
	$\cdots\uparrow\downarrow\circ \ \uparrow\circ \ \downarrow\circ \ \ \circ \ \cdots$	3W	
$\frac{U}{t} \approx \frac{W}{t} \ll 1$	$\cdots\uparrow\downarrow\circ \ \uparrow\circ \ \downarrow\circ \ \ \circ \ \cdots$	-t	
	$\cdots \uparrow\circ \ \ \circ \ \uparrow\downarrow\circ \ \downarrow\circ \ \cdots$	-t	no

Table 1.1: extended Hubbard describing electrons on an atomic string

While the ground state configuration for the last two cases is quite intuitive, the arrangement of the electrons for $W = 0$ and $\frac{U}{t} \gg 1$ is less trivial. For this situation the hopping term can be described in form of a perturbation. Then the according unperturbed ground state has no twofold occupations of lattice sites. Nevertheless, still many different configurations, with only one electron per site are possible. Turning on a small perturbation t, however favors an anti ferromagnetic configuration, as this still allows virtual hopping processes. These are processes, where an electron hops from one site to the neighboring and back, leading to a reduction of the energy $\propto -\frac{t^2}{U}$. Electrons on neighboring sites, with parallel orientated spins, cannot perform these virtual hoppings as they are restricted by the Pauli principle.

Summarizing, this means that U triggers anti-ferromagnetic ordering, where spin-up and spin-down electrons appear alternately (also known as spin-density wave SDW), whereas W prefers a charge ordering, where the electrons doubly occupy every second site (i.e., charge-density wave CDW). But as long as both are small compared to t no ordering will happen.

To go from a qualitative picture to a quantitative one, one needs to actually solve the Schrödinger equation, but by looking at equation (1.20) we encounter a last remaining problem. As the kinetic energy term becomes diagonal in reciprocal space and the potential energy term in real space, a simultaneous diagonalization is difficult, and we need to make further approximations. In this thesis, two approaches are applied and compared to each other, namely mean-field (MFT) and dynamical mean-field theory (DMFT). MFT is a rather simple method which neglects quantum fluctuations, but still often suites to get a qualitative idea, whereas DMFT recovers fluctuations locally and gives a more accurate result. Both methods and the respective results are discussed and shown in the following two sections.

1.3   Mean Field Theory

A typical illustration of the classical mean field theory is the application to the Ising model:

$$H = -h \sum_i S_i - \sum_{(ij)} J_{ij} S_i S_j \tag{1.22}$$

with i and j again labeling the lattice site. Unless there exist exact solutions for 1D and 2D lattices (strictly speaking: just for $j = i + 1$), one has to make approximations for three dimensions. For MFT this means finding an effective non-interacting Hamiltonian in the form of:

$$H_{eff} = -\sum_i h_i^{eff} S_i \tag{1.23}$$

with the (Weiss) effective field h_i^{eff} and the single-site spin-operator S_i. The crucial idea now is to choose h_i^{eff} such that the magnetization is reproduced accurately, meaning

$$
\begin{aligned}
m_i &= \langle S_i \rangle \\
&= \frac{1}{Z} \sum_n \langle n | e^{-\beta H_{eff}} S_i | n \rangle \\
&= \frac{1}{Z} \sum_n \langle n | e^{\sum_i h_i^{eff} S_i} S_i | n \rangle .
\end{aligned}
\tag{1.24}
$$

As there are just two possible eigenstates $|\uparrow\rangle$ and $|\downarrow\rangle$ with

$$
\begin{aligned}
S_i |\uparrow\rangle &= |\uparrow\rangle \\
S_i |\downarrow\rangle &= - |\downarrow\rangle .
\end{aligned}
\tag{1.25}
$$

the normalisation becomes

$$Z = e^{+\beta h_{eff}} \langle \uparrow | \uparrow \rangle + e^{-\beta h_{eff}} \langle \downarrow | \downarrow \rangle = 2 \cdot \cosh(\beta h_i^{eff}). \tag{1.26}$$

Evaluating the expectation value of (1.24) in this local two-state basis gives

$$m_i = \frac{\sinh(\beta h_i^{eff})}{\cosh(\beta h_i^{eff})} = \tanh(\beta h_i^{eff}) \tag{1.27}$$

Thus we define the condition h_i^{eff} needs to fulfill,

$$\beta h_i^{eff} = \tanh^{-1}(m_i). \tag{1.28}$$

So far everything is exact, but to get a hamiltonian in the form of eq. (1.23) one has to neglect fluctuation terms (mean-field approximation)

$$(S_i - \langle S_i \rangle)(S_j - \langle S_j \rangle) \stackrel{!}{\approx} 0, \tag{1.29}$$

so it follows that

$$S_i S_j = S_j \langle S_i \rangle) + S_i \langle S_j \rangle) - \langle S_i \rangle \langle S_j \rangle. \tag{1.30}$$

The last term in eq. (1.30) is not relevant, as it again just gives a constant to the Hamiltonian, which now reads

$$H = -h \sum_i S_i - \sum_{(ij)} J_{ij}(S_j \langle S_i \rangle + S_i \langle S_j \rangle) \tag{1.31}$$

With eq. (1.23) and (1.30) one now has an expression for the (Weiss) effective field. If we further consider isotropy ($J_{ij} = J$, $m_i = m$) and $J > 0$ (ferromagnetic solution) one gets

$$h_i^{eff} = h^{eff} = h + zJm. \tag{1.32}$$

Finally, we have the self-consistency equation

$$m = \tanh(\beta(h + zJm)) \tag{1.33}$$

which can be solved graphically.

A more general approach, when one cannot write the problem in terms of $m = f(m)$, is to solve the problem iteratively. One therefore starts with a value m_0, as an initial guess for the true m, and calculate h_{eff} with eq. (1.32). Eq. 1.24 then gives a new guess m_1, which is used to calculate h_{eff} again etc... This procedure is repeated until convergence is reached, i.e., the values of m for two consecutive iterations l and $l+1$ do not differ more than a small tolerance value ϵ_{tol}

$$|m_l - m_{l+1}| < \epsilon_{tol}. \tag{1.34}$$

1.3.1 Mixing

Numerical instabilities can slow down extremely or even destroy convergence. Simple mixing is the easiest way to overcome this problem. Therefore the self-consistency parameter of iteration $i + 1$ gets mixed with the one of iteration i, i.e., one replaces

$$m_{i+1} \tag{1.35}$$

by

$$p \cdot m_{i+1} + (1 - p) \cdot m_i, \tag{1.36}$$

where p takes a value between 1 and 0. $p = 1$ means no further solution is mixed in and may lead to instabilities, whereas $p \ll 1$ obviously convergences too slow. Typically p around 0.7 gives the fastest possible convergence.

1.3.2 Application of MFT to the extended Hubbard Model

To treat eq. (1.20) in a mean-field way the two Coulomb-interaction terms need to be approximated. The easiest way to do so is to take the mean value of the particle density $\langle n_{i\sigma}^c \rangle$ as control parameter and again neglect fluctuation terms similar to eq. (1.30). Before applying MFT to the on-site interaction term we initially need to rewrite as

$$U \sum_i n_{i\uparrow} n_{i\downarrow} = \frac{U}{2} \sum_{i\sigma} n_{i\sigma} n_{i\bar{\sigma}}. \tag{1.37}$$

Further we write the particle operators in terms of the average value plus a fluctuation operator

$$
\begin{aligned}
&\frac{U}{2} \sum_{i\sigma} \left(\langle n_{i\bar{\sigma}} \rangle + \delta n_{i\sigma} \right) \left(\langle n_{i\bar{\sigma}} \rangle + \delta n_{i\bar{\sigma}} \right) \\
&= \frac{U}{2} \sum_{i\sigma} \langle n_{i\sigma} \rangle \langle n_{i\bar{\sigma}} \rangle + \delta n_{i\sigma} \langle n_{i\bar{\sigma}} \rangle + \delta n_{i\bar{\sigma}} \langle n_{i\sigma} \rangle + \underbrace{\delta n_{i\bar{\sigma}} \delta n_{i\sigma}}_{\approx 0}
\end{aligned}
\tag{1.38}
$$

and neglect, in a similar manner as in eq. (1.30), the fluctuation-fluctuation term. To restore an expression without fluctuation terms we again use:

$$\delta n_{i\sigma} = (n_{i\sigma} - \langle n_{i\sigma} \rangle) \tag{1.39}$$

and obtain

$$\frac{U}{2} \sum_{i\sigma} n_{i\sigma} n_{i\bar\sigma} \approx \frac{U}{2} \sum_{i\sigma} \left(n_{i\sigma} \langle n_{i\bar\sigma} \rangle + n_{i\bar\sigma} \langle n_{i\sigma} \rangle - \langle n_{i\sigma} \rangle \langle n_{i\bar\sigma} \rangle \right) \tag{1.40}$$

as the two terms in the sum describe the same it follows that

$$U \sum_{i} n_{i\uparrow}^{c} n_{i\downarrow}^{c} \approx U \sum_{i,\sigma} n_{i\sigma}^{c} \langle n_{i\bar\sigma}^{c} \rangle - \langle n_{i\uparrow}^{c} \rangle \langle n_{i\downarrow}^{c} \rangle . \tag{1.41}$$

Similar to eq. (1.40), one gets for the nearest neighbor interaction term

$$W \sum_{\langle ij \rangle} n_i n_j \approx W \sum_{\langle ij \rangle,\sigma} n_{i\sigma} \langle n_j \rangle + n_{j\sigma} \langle n_i \rangle - \langle n_i \rangle \langle n_j \rangle \tag{1.42}$$

1.3.3 The honeycomb lattice
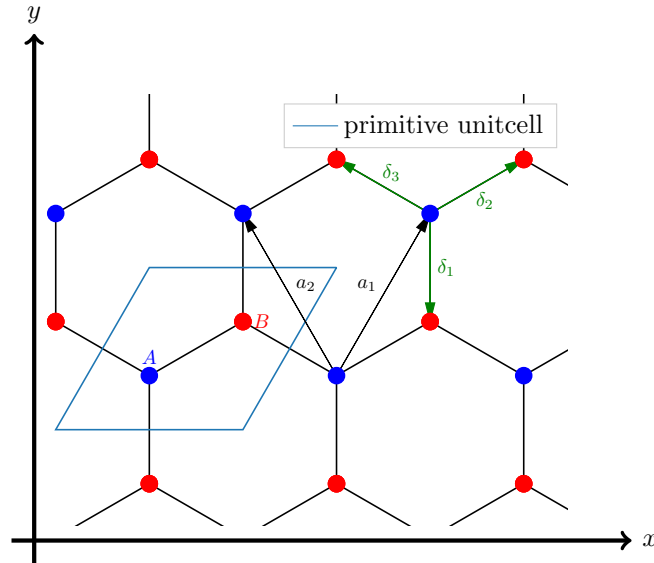
Figure 1.1: Honeycomb lattice

The honeycomb lattice as shown in figure 1.1 is a two dimensional hexagonal crystal structure with two atoms in the basis (here denoted as A and B). Every translation vector $\mathbf{t}$ of the crystal can be written in terms of two primitive lattice vectors

$$\mathbf{t} = l_1 \mathbf{a_1} + l_2 \mathbf{a_2} \tag{1.43}$$

with l_1 and l_2 being integer values and

$$\mathbf{a_1} = \frac{a}{2} \begin{pmatrix} 1 \\ \sqrt{3} \end{pmatrix} , \quad \mathbf{a_2} = \frac{a}{2} \begin{pmatrix} -1 \\ \sqrt{3} \end{pmatrix} \tag{1.44}$$

being the primitive lattice vectors with the lattice parameter a as their length. The vectors $\delta_1, \delta_2, \delta_3$ connecting two neighboring atoms A and B further read

$$\delta_1 = \frac{a}{\sqrt{3}} \begin{pmatrix} 0 \\ -1 \end{pmatrix} , \quad \delta_2 = \frac{a}{2\sqrt{3}} \begin{pmatrix} \sqrt{3} \\ 1 \end{pmatrix} , \quad \delta_3 = \frac{a}{2\sqrt{3}} \begin{pmatrix} -\sqrt{3} \\ 1 \end{pmatrix} . \tag{1.45}$$

Using the basis (1.44), we find the reciprocal lattice vectors $\mathbf{b_1}$ and $\mathbf{b_2}$

$$\mathbf{b_1} = \frac{2\pi}{a\sqrt{3}} \begin{pmatrix} \sqrt{3} \\ 1 \end{pmatrix} , \quad \mathbf{b_2} = \frac{2\pi}{a\sqrt{3}} \begin{pmatrix} -\sqrt{3} \\ 1 \end{pmatrix} . \tag{1.46}$$

The according Brillouin zone is drawn in figure 1.2, with the following high-symmetry points:

$$\mathbf{\Gamma} = \begin{pmatrix} 0 \\ 0 \end{pmatrix} , \quad \mathbf{M} = \frac{\pi}{a\sqrt{3}} \begin{pmatrix} \sqrt{3} \\ 1 \end{pmatrix} , \quad \mathbf{K} = \frac{2\pi}{3a} \begin{pmatrix} 1 \\ \sqrt{3} \end{pmatrix}$$

$$\mathbf{M'} = \frac{2\pi}{a\sqrt{3}} \begin{pmatrix} 0 \\ 1 \end{pmatrix} , \quad \mathbf{K'} = \frac{2\pi}{3a} \begin{pmatrix} -1 \\ \sqrt{3} \end{pmatrix} \tag{1.47}$$
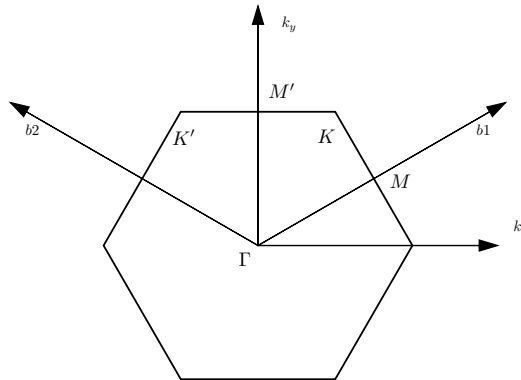
Figure 1.2: Honeycomb lattice in reciprocal space

We now split the total Hamiltonian in three parts, one k-dependent kinetic energy term including nearest-neighbor hopping and the two interaction terms:

$$H(\mathbf{k}) = H'(\mathbf{k}) + H_U + H_V \tag{1.48}$$

To evaluate the Hamiltonian resulting from equation (1.20) in the approximation of (1.41) and (1.42) we first consider the tight-binding Hamiltonian (hopping-term)

$$H_{TB} = -t \sum_{\langle ij \rangle, \sigma} (a_{i\sigma}^\dagger b_{j\sigma} + h.c.), \tag{1.49}$$

where $b_{j\sigma}$ destroys an electron with spin σ on the sublattice B and $a_{i\sigma}^\dagger$ creates the same electron on sublattice A. As the Hamiltonian does not depend on the spin it is sufficient to evaluate just the term

$$-t \sum_{\langle ij \rangle} a_i^\dagger b_j = -t \sum_i (a_i^\dagger b_{i+n1} + a_i^\dagger b_{i+n2} + a_i^\dagger b_{i+n3}) \tag{1.50}$$

where $n1$ labels the nearest-neighbor atom the electron is coming from (going to). For instance $a_i^\dagger b_{i+n1}$ stands for an electron hopping from atom B at lattice-site position $\mathbf{r}_i + \delta_1$ to atom A at position $\mathbf{r}_i$ etc. This term is evaluated by exploiting the fact that a periodic crystal structure is assumed, which allows us to rewrite the construction and annihilation operators as a fourier series:

$$c_i = \frac{1}{\sqrt{N}} \int_{BZ} c_k e^{-i\mathbf{k}\mathbf{r_i}} \tag{1.51}$$

Taking this definition and its hermitian conjugate respectively leads to

$$
\begin{aligned}
H_{TB} &= -t \sum_i \frac{1}{N} \int_{BZ(\mathbf{k})} \int_{BZ(\mathbf{k}')} a_{\mathbf{k}}^\dagger e^{i\mathbf{k}\mathbf{r_i}} b_{\mathbf{k}'} e^{-i\mathbf{k}'(\mathbf{r_i}+\delta_1)} + ... \\
&= -t \sum_i \frac{1}{N} \int_{BZ(\mathbf{k})} \int_{BZ(\mathbf{k}')} a_{\mathbf{k}}^\dagger b_{\mathbf{k}'} \underbrace{e^{i(\mathbf{k}-\mathbf{k}')\mathbf{r_i}}}_{\delta(\mathbf{k}-\mathbf{k}')} e^{-i\mathbf{k}'\delta_1} + ... \\
&= -t \underbrace{\sum_i \frac{1}{N}}_{1} \int_{BZ(\mathbf{k})} a_{\mathbf{k}}^\dagger b_{\mathbf{k}} e^{-i\mathbf{k}\delta_1} + ... \\
&= -\int_{BZ(\mathbf{k})} g_{\mathbf{k}}\, a_{\mathbf{k}}^\dagger b_{\mathbf{k}} + h.c.
\end{aligned}
$$

With eq. (1.45) we find

$$g_{\mathbf{k}} = t \left[e^{i\frac{ak_y}{\sqrt{3}}} + 2\cos\left(\frac{ak_x}{2}\right) e^{-i\frac{ak_y}{2\sqrt{3}}} \right]. \tag{1.52}$$

Taking the basis set as $\Psi_{\mathbf{k}}^{\dagger} = \left(a_{\mathbf{k},\uparrow}^{\dagger}, b_{\mathbf{k},\uparrow}^{\dagger}, a_{\mathbf{k},\downarrow}^{\dagger}, b_{\mathbf{k},\downarrow}^{\dagger} \right)$, the tight-binding term in matrix representation can be written as

$$H_{TB} := H'(\mathbf{k}) = \begin{pmatrix} 0 & -g_{\mathbf{k}} & 0 & 0 \\ -g_{\mathbf{k}}* & 0 & 0 & 0 \\ 0 & 0 & 0 & -g_{\mathbf{k}} \\ 0 & 0 & -g_{\mathbf{k}}* & 0 \end{pmatrix}, \tag{1.53}$$

containing two independent and identical spin-blocks.

Using again equation (1.51) to rewrite the interaction term in mean-field approximation (equation (1.41) without constant terms), we get

$$\begin{aligned} H_U &= \sum_{i,\sigma} \left(a_{i,\sigma}^{\dagger} a_{i,\sigma} \langle n_{A\bar{\sigma}} \rangle + b_{i,\sigma}^{\dagger} b_{i,\sigma} \langle n_{B\bar{\sigma}} \rangle \right) \\ &= \sum_{\sigma} \int_{BZ} \left(a_{\mathbf{k},\sigma}^{\dagger} a_{\mathbf{k},\sigma} \langle n_{A\bar{\sigma}} \rangle + b_{\mathbf{k},\sigma}^{\dagger} b_{\mathbf{k},\sigma} \langle n_{B\bar{\sigma}} \rangle \right)' \end{aligned} \tag{1.54}$$

resulting in the matrix representation

$$H_U = U \begin{pmatrix} \langle n_{A\downarrow} \rangle & 0 & 0 & 0 \\ 0 & \langle n_{B\downarrow} \rangle & 0 & 0 \\ 0 & 0 & \langle n_{A\uparrow} \rangle & 0 \\ 0 & 0 & 0 & \langle n_{B\uparrow} \rangle \end{pmatrix}. \tag{1.55}$$

Similarly the inter-site interaction term becomes

$$H_V = \underbrace{zW}_{V} \begin{pmatrix} \langle n_B \rangle & 0 & 0 & 0 \\ 0 & \langle n_A \rangle & 0 & 0 \\ 0 & 0 & \langle n_B \rangle & 0 \\ 0 & 0 & 0 & \langle n_A \rangle \end{pmatrix}, \tag{1.56}$$

where z gives the coordination number (i.e., the number of nearest neighboring atoms, which is $z = 3$ for the honeycomb lattice). At this point we define the product of

zW as the total nearest-neighbor interaction V and will from now on only use V as a parameter for nearest neighbor interactions.

As for numerical reasons we need to approximate the integral over the Brillouine zone $\int_{BZ}$ by a finite sum of $\mathbf{k}$- point $\sum_{\mathbf{k}}$ the total mean-field Hamiltonian states

$$H_{\text{MFT}} = \frac{1}{N_\Lambda} \sum_{\mathbf{k}} \Psi_{\mathbf{k}}^\dagger \left(H'(\mathbf{k}) + H_U + H_V \right) \Psi_{\mathbf{k}} - c\cdot, \tag{1.57}$$

with the number of $\mathbf{k}$-points N_Λ and a constant energy shift c coming from (1.40) and (1.42),

$$c = \left(\langle n_{A\downarrow} \rangle \langle n_{A\uparrow} \rangle + \langle n_{B\downarrow} \rangle \langle n_{B\uparrow} \rangle \right) + \langle n_B \rangle \langle n_A \rangle . \tag{1.58}$$

This energy-shift for now does not need to be considered, but will become important for the calculation of the total energy later.

1.3.4 Self-consistency condition

The expectation values for the density $\langle n_{A\downarrow} \rangle$, $\langle n_{A\uparrow} \rangle$, $\langle n_{B\downarrow} \rangle$, $\langle n_{B\uparrow} \rangle$ determine the Hamiltonian of equation (1.57). On the other hand, theses expectation values are given by the occupied eigenstates $u_{m\mathbf{k}}$ with the energy $e_{m\mathbf{k}}$ as

$$\langle n_{o\sigma} \rangle = \sum_{\mathbf{k},m} \Theta \left(\mu - e_{m\mathbf{k}} \right) \left| u_{m\mathbf{k}}^o \right|^2 \tag{1.59}$$

where o labels the different atom types A and B, and μ is the chemical potential, which needs to be chosen such that half filling is assured. Due to the particle-hole symmetry of the (extended) Hubbard model the chemical potential can be found a priori in the case of half-filling.

1.3.5 Particle-hole symmetry and chemical potential at half filling

We may consider an operator which exchanges the role of creation and annihilation. A creation operator $c_{i\sigma}^\dagger$ of a fermionic particle (obeying the anti-commutation relations of equation (1.10)) hence can be replaced by a destruction operator $d_{i\sigma}$ of a hole (obeying the same anti-commutation relations). For a bipartite lattice like the honeycomb-lattice

the following particle-hole transformation can be done [5]

$$c_{i\sigma}^{\dagger} = \begin{cases} -d_{i\sigma} & \text{for sublattice } A \\ d_{i\sigma} & \text{for sublattice } B \end{cases} \tag{1.60}$$

Applying this transformation on the kinetic energy term of equation (1.20) leaves the form unchanged

$$c_{i\sigma}^{\dagger} c_{j\sigma} \rightarrow -d_{i\sigma} d_{j\sigma}^{\dagger} = d_{j\sigma}^{\dagger} d_{i\sigma}, \tag{1.61}$$

for i and j belonging to different sublattices (which is the case for nearest-neighbor hopping).

On the other hand, diagonal terms (density operators), as we can find them in both other potential energy terms, will transform as

$$n_{i\sigma}^{c} = c_{i\sigma}^{\dagger} c_{i\sigma} \rightarrow d_{i\sigma} d_{i\sigma}^{\dagger} = 1 - \underbrace{d_{i\sigma}^{\dagger} d_{i\sigma}}_{=n_{i\sigma}^{d}} \tag{1.62}$$

So if the filling given by $n_{i\sigma}^{c}$ equals one, the filling of $n_{i\sigma}^{d}$ becomes zero and the other way around. If we rewrite the on-site and the nearest-neighbor interaction in the following form

$$U \sum_{i} \left(n_{i\uparrow}^{c} - \frac{1}{2} \right) \left(n_{i\downarrow}^{c} - \frac{1}{2} \right) + W \sum_{\langle ij \rangle} \left(n_{i}^{c} - 1 \right) \left(n_{j}^{c} - 1 \right), \tag{1.63}$$

this term becomes also symmetric to the transformation of equation (1.60), just as the kinetic energy term. Expanding equation (1.63) results in the previous form of the interaction terms plus a trivial shift in the chemical potential and an overall constant energy

$$U \sum_{i} n_{i\uparrow}^{c} n_{i\downarrow}^{c} + W \sum_{\langle ij \rangle} n_{i}^{c} n_{j}^{c} - \left(\frac{U}{2} + V \right) \sum_{i} n_{i}^{c} + \frac{U}{2} + V, \tag{1.64}$$

where again the above definition of $zW = V$ was used. But as no chemical potential was used until now this gives us the definition of the chemical potential that ensures half-filling and particle-hole symmetry:

$$\mu = \frac{U}{2} + V \tag{1.65}$$

In the following sections the parameter t was set to one, and the interaction parameters U and V as well as the energy, are given in units of t.

1.3.6 Results

For all calculations in this section the following parameters were chosen:

- At least 400 **k**-points in the Brillouin zone to approximate the density of states of a infinite crystal. For higher numbers of **k**-points the critical transition values do not change significantly (i.e., in the order of 10^{-3}).

- A tolerance of $\epsilon_{tol} \geq 10^{-4}$.

- A mixing of the particle densities between 0.9 and 0.7.

For the tight-binding Hamiltonian without interaction we find the conduction and valence band intersect at the two high-symmetry K points (see figure 1.3). The linearity of the dispersion relation around these points makes a corresponding electron behave like a massless particle. The dispersion around K and K' are called Dirac-cones.
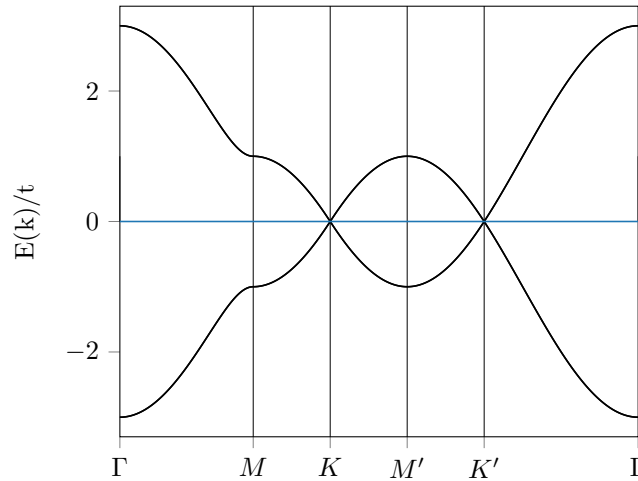
Figure 1.3: Dispersion relation for $V = U = 0$

Only on-site interaction (SDW-transition)

For the quantification of the SDW-order, the anti-ferromagnetic order parameter M_{AF} is defined as

$$M_{AF} = -\langle n_{A\uparrow}\rangle + \langle n_{A\downarrow}\rangle + \langle n_{B\uparrow}\rangle - \langle n_{B\downarrow}\rangle. \tag{1.66}$$

As the sum over the densities $\sum_{o,\sigma} \langle n_{o,\sigma} \rangle$ must give two (due to half filling), M_{AF} will be in the range of $[-2, 2]$. But as exchanging A and B changes the sign of M_{AF} and still is an equivalent expression, we will just consider positive values of M_{AF} and refrain from using $|M_{AF}|$ in figures an descriptions.

To investigate the transition to anti-ferromagnetic ordering we continuously change the interaction U and evaluated a self-consistent solution using equation (1.59) taking a density distribution $\langle n_{o,\sigma} \rangle$ corresponding to a finite value of M_{AF} as initial parameters. To guarantee fast convergence, calculations were performed starting from strong interactions and going over to lower ones using the previous solution of M_{AF} as a new starting parameter.

We can gather from figure 1.4 that a gap opens up and anti-ferromagnetic ordering appears above a critical value $U_c =2.23t$. This value is consistent with existing literature [6].
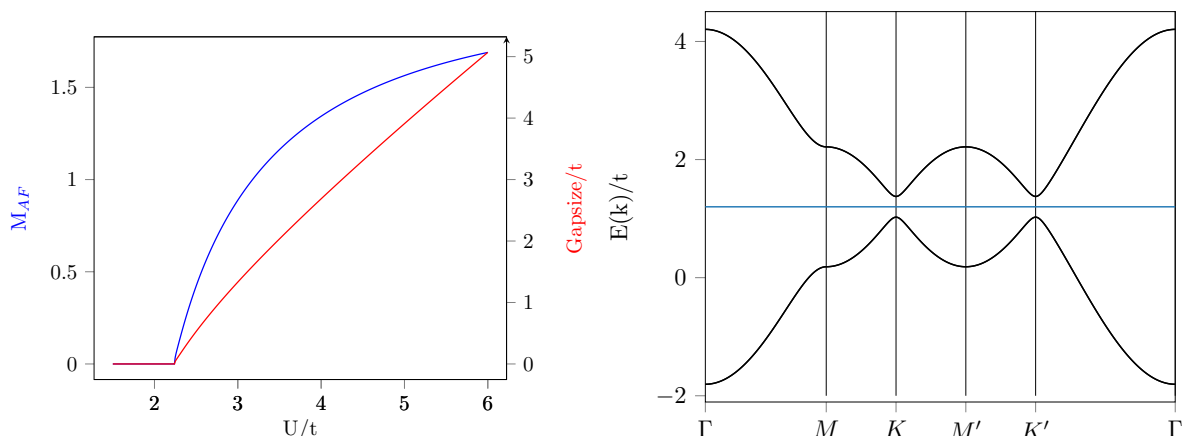
Figure 1.4: SDW-transition (left) and dispersion relation for $U = 2.4t$, $V = 0$ (right)

Only nearest neighbor interaction (CDW-transition)

Similar to the above situation we can define a charge ordering parameter

$$\Delta_{AB} = - \langle n_{A\uparrow} \rangle - \langle n_{A\downarrow} \rangle + \langle n_{B\uparrow} \rangle + \langle n_{B\downarrow} \rangle, \tag{1.67}$$

quantifying the CDW phase. With a similar discussion as for M_{AF}, Δ_{AB} is restricted to values between $[-2, 2]$, but it is sufficient to consider just positive values.

For the transition a critical value of $V_c = 1.12t$ is found.
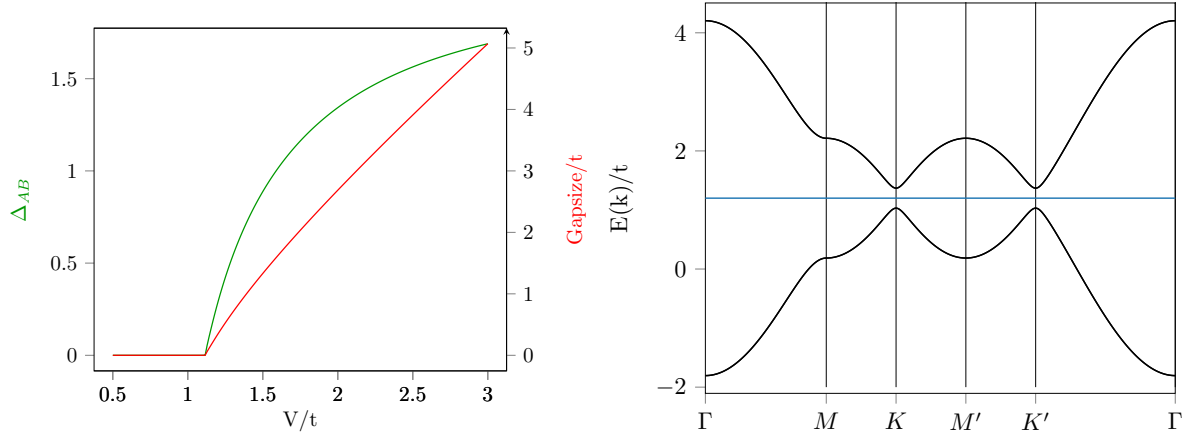
Figure 1.5: CDW-transition (left) and dispersion relation for $U = 0$, $V = 1.12t$ (right)

Comparing figure 1.4 and 1.5 we see a similar behavior of the two transition types. This will be further discussed in a more general way also including spin-orbit coupling in section 2.3.1.

Interplay between the different phases

To investigate the interplay between on-site and nearest-neighbor interaction, respectively, SDW and CDW calculations were performed for different sets of V and U. Hereby we find that the critical value U_c is independent of V, whereas U seems to reduce the effective nearest-neighbor interaction:

$$V_{\text{eff}} = V - \frac{U}{2} \tag{1.68}$$

Between CDW and SDW we find a first order transition at $U = V$. (this can also be shown analytically and will be further discussed together with spin-orbit coupling)
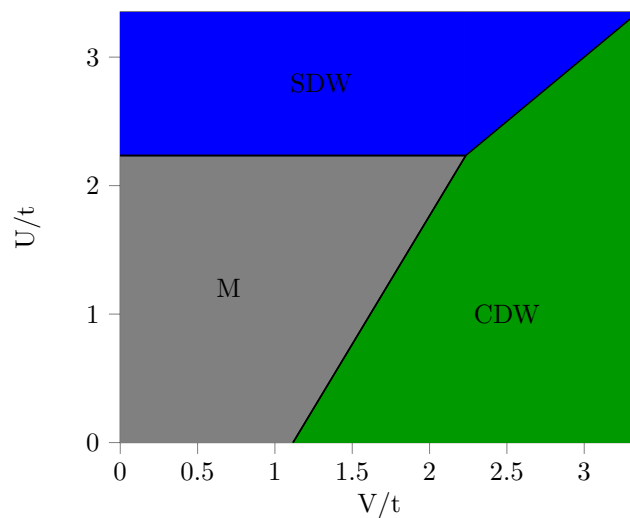
Figure 1.6: Phase diagram using MFT, M ... metallic phase (unordered), SDW ... spin density wave, CDW ... charge density wave

Apart from the three phases already known from the general extreme cases considered for an atomic chain (see table 1.1) no other phases are found. Independently from the initial parameters $\langle n_{o,\sigma} \rangle$ always one of these phases is found self-consistently. There are no ferromagnetic solutions, i.e.

$$\langle n_{A\uparrow} \rangle + \langle n_{B\uparrow} \rangle = \langle n_{A\downarrow} \rangle + \langle n_{B\downarrow} \rangle \tag{1.69}$$

is always valid. Besides we can find no stable mixed solution of CDW and SDW, so either Δ_{AB} or M_{AF} is always zero, whenever the other order parameter is finite.

1.4 Dynamical Mean Field Theory

The following pages follow mainly [7]. The dynamical mean-field theory (DMFT) is the quantum generalization of mean-field theory. This means that for the (Weiss) effective field of the model also local quantum fluctuations are considered. Moreover the local problem is treated as an exact manybody interaction problem. The crucial idea of DMFT is to replace a lattice model by a single site coupled to a self-consistent bath (see figure 1.7), where the bath has the role of an effective field. The central quantity used in DMFT calculations is the local (lattice) Green's function
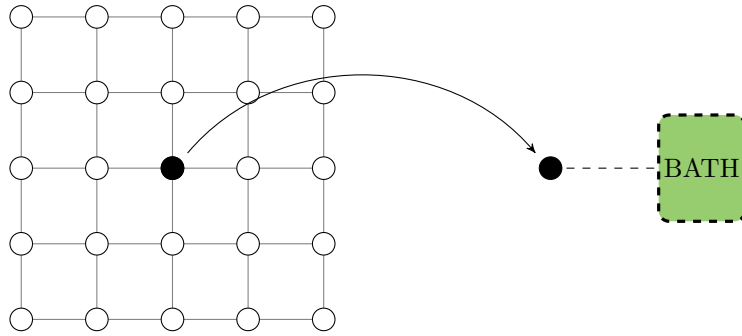
Figure 1.7: Idea of Mean-filed theory: replace a lattice problem by an impurity problem

$$\mathcal{G}_{loc}^{\sigma}\left(\tau - \tau'\right) \equiv - \left\langle T c_{i\sigma}(\tau) c_{i\sigma}^{\dagger}(\tau') \right\rangle \tag{1.70}$$

We take again the simple Hubbard model with single-orbital atoms (1.18) as example for our lattice model. Additionally we now need to introduce an impurity model which describes a single atom coupled to an effective bath. In case of the Hubbard model this would be the Anderson impurity model (AIM [8])

$$H_{AIM} = H_{atom} + H_{coupling} + H_{bath} \tag{1.71}$$

here the site index for the impurity orbital $c_{\sigma}^{\dagger}$ is dropped for simplicity reasons with:

$$H_{atom} = U n_{i\uparrow}^{c} n_{i\downarrow}^{c} + (\epsilon_0 - \mu) \left(n_{i\uparrow}^{c} + n_{i\downarrow}^{c} \right)$$
$$H_{coupling} = \sum_{k,\sigma} V_k \left(a_{k\sigma}^{\dagger} c_\sigma + c_\sigma^{\dagger} a_{k\sigma} \right)$$
$$H_{bath} = \sum_{k,\sigma} \tilde{\epsilon}_k a_{k\sigma}^{\dagger} a_{k\sigma}$$

where the first term describes the on-site interaction of the electron, with U being the interaction of two electrons within an orbital. The second term gives the coupling (or hybridization) with the bath, where the $a_{k\sigma}^\dagger$'s are the non-interacting fermions of the effective bath and the V_k's are the hopping amplitudes of electrons hopping from the bath to the impurity site and back. The bath Hamiltonian consists just of the effective non-interacting electron energies $\tilde{\epsilon}_k$, which should not be confused with the electron energies of the lattice model ϵ_k.

The impurity Green's function $\mathcal{G}_{imp}$ can now be written in the form of a Feynman path integral

$$\mathcal{G}_{imp}(\tau - \tau') = \frac{1}{Z} \int D[\hat{c}_\sigma^\dagger, \hat{c}_\sigma] \hat{c}_\sigma^\dagger(\tau') \hat{c}_\sigma(\tau) e^{S_{eff}}, \tag{1.72}$$

depending on an effective action

$$S_{eff} = -\sum_\sigma \int_0^\beta d\tau \int_0^\beta d\tau' \hat{c}_\sigma^\dagger(\tau) \left(\mathcal{G}_{imp}^0(\tau - \tau') \right)^{-1} \hat{c}_\sigma(\tau') + U \int_0^\beta d\tau \hat{n}_\uparrow^c(\tau) \hat{n}_\downarrow^c(\tau) \tag{1.73}$$

for the impurity orbital, which represents the effective dynamics of the local site. Hereby $\mathcal{G}_{imp}^0(\tau - \tau')$ describes the bare propagation of an electron created at imaginary time τ on the lattice site (coming from the bath) and destroyed at a later imaginary time τ' (going back to the bath).

This effective non-interacting Green's function is also referred to as dynamic Weiss-field, as it is the quantum generalization of the mean-field effective field and can directly be obtained by solving the (Fourier transformed) time-dependent Schrödinger equation

$$(i\omega_n - T)\mathscr{G}_{imp}^0(i\omega_n) = \mathbf{1} \tag{1.74}$$

in which T is equal to the H_{AIM} without the U-term and $\mathscr{G}_{imp}^0(i\omega_n)$ gives the full free Green's function of the AIM including the bath degrees of freedom.

Due to the periodicity of $\mathcal{G}_{imp}^0(\tau - \tau')$, this so called Matsubara Green's function is defined for discrete (but infinitely many) Matsubara frequencies

$$\omega_n = \frac{(2n + 1)}{\beta} \tag{1.75}$$

depending on the inverse temperature β and an integer n. By integrating out the

non-interacting bath degrees of freedom one can derive the following expression

$$\left(\mathcal{G}^0_{imp}(i\omega_n)\right)_{00} := \mathcal{G}^0_{imp}(i\omega_n) = \frac{1}{i\omega_n + \mu - \epsilon_0 - \Delta(i\omega_n)} \tag{1.76}$$

$$\Delta(\omega_n) = \sum_k \frac{|V_k|^2}{i\omega_n - \tilde{\epsilon}_k}.$$

As one can see the V_k's and $\tilde{\epsilon}_k$'s are now only entering through the so called hybridization function $\Delta(i\omega)$.

The equation of motion for a general interacting Hamiltonian can effectively be written in form of a Dyson equation

$$\mathcal{G}(\mathbf{k}, i\omega_n) \equiv \left(\left(\mathcal{G}^0(\mathbf{k}, i\omega_n)\right)^{-1} - \Sigma(\mathbf{k}, i\omega_n)\right)^{-1} \tag{1.77}$$

where $G(\mathbf{k}, i\omega)$ gives the full interacting Green's function and $\Sigma(\mathbf{k}, i\omega)$ the so called self-energy which represents the interaction.

This lets us write the lattice Green's function in the following form:

$$\mathcal{G}(\mathbf{k}, i\omega_n) = \frac{1}{i\omega_n + \mu - \epsilon_0 - \epsilon_{\mathbf{k}} - \Sigma(\mathbf{k}, i\omega_n)} \tag{1.78}$$

in which $\epsilon_{\mathbf{k}}$ is the Fourier transform of the hopping integral t_{ij}.

Now, DMFT approximation comes into the play,

$$\begin{aligned} \Sigma(\mathbf{k}, i\omega_n) &\approx \Sigma(i\omega_n) \\ \Sigma(i\omega_n) &\approx \Sigma_{imp}(i\omega_n), \end{aligned} \tag{1.79}$$

which means we neglect all non-local terms of the lattice self-energy and approximate the local terms by the impurity self-energy $\Sigma_{imp}(i\omega_n)$

Replacing $\Sigma(\mathbf{k}, i\omega_n)$ by $\Sigma_{imp}(i\omega_n)$ in eq. (1.78) and rewriting the impurity self-energy according to the Dyson equation (1.77) gives the lattice Green's function in terms of the impurity Green's function. By subsequently summing over $\mathbf{k}$ one obtains the local lattice Green's function,

$$\mathcal{G}_{loc}(i\omega_n) = \sum_{\mathbf{k}} \frac{1}{\Delta(i\omega_n) + \mathcal{G}_{imp}(i\omega_n)^{-1} - \epsilon_{\mathbf{k}}}, \tag{1.80}$$

which by construction must coincide with the impurity Green's function

$$\mathcal{G}_{loc}(i\omega_n) \overset{!}{=} \mathcal{G}_{imp}(i\omega_n). \tag{1.81}$$

Equation (1.80) and (1.81) define the self-consistency condition of DMFT. The correct choice of the V_k's and the $\tilde{\epsilon}_k$'s will be reached when the two local Green's functions of both models coincide. The only thing left from the original model here are the hopping amplitudes $\epsilon_{\mathbf{k}}$. To get a computational more practical term one can now replace the $\epsilon_{\mathbf{k}}$ by a continues variable $\epsilon_{\mathbf{k}}$ and multiply by the density of states

$$D(\epsilon) \equiv \sum_{\mathbf{k}} \delta \left(\epsilon - \epsilon_{\mathbf{k}} \right), \tag{1.82}$$

which leads to

$$\mathcal{G}_{loc}(i\omega_n) = \int d\epsilon \frac{1}{\Delta(i\omega_n) + \mathcal{G}_{imp}(i\omega_n)^{-1} - \epsilon} \tag{1.83}$$

1.4.1 The self-consistency loop

The only two necessary input parameters for DMFT are

- the density of states $D(\epsilon)$ of the non-interacting lattice model

- the on-site interaction parameter U

Given that, the self-consistency loop in its simplest form is performed as shown in figure 1.8 by

1. making an **initial guess for the self-energy**. This will usually be zero (unless we know better).

2. plugging the result into the modified **'Dyson equation'** $(\mathcal{G}^0_{imp})^{-1} = (\mathcal{G}_{loc})^{-1} + \Sigma$ to **obtain** a **non-interacting impurity Green's function**. This will become a real Dyson equation in the end when $\mathcal{G}_{imp} = \mathcal{G}_{loc}$ is fulfilled.

3. calculating the **impurity Green's function** by using an appropriate **impurity solver** $\Gamma(\mathcal{G}^0_{imp}, U)$ to estimate the Feynman path integral of equation (1.72).

4. **comparing** $\mathcal{G}_{imp}$ and $\mathcal{G}_{loc}$.

5. if $\mathcal{G}_{imp}$ and $\mathcal{G}_{loc}$ differ less than a chosen tolerance ϵ_{tol} DMFT is **converged**. **Otherwise** we go **back** to 2.

add 5. : In practice one should also check if the self-energy remains unchanged from one iteration to the following!
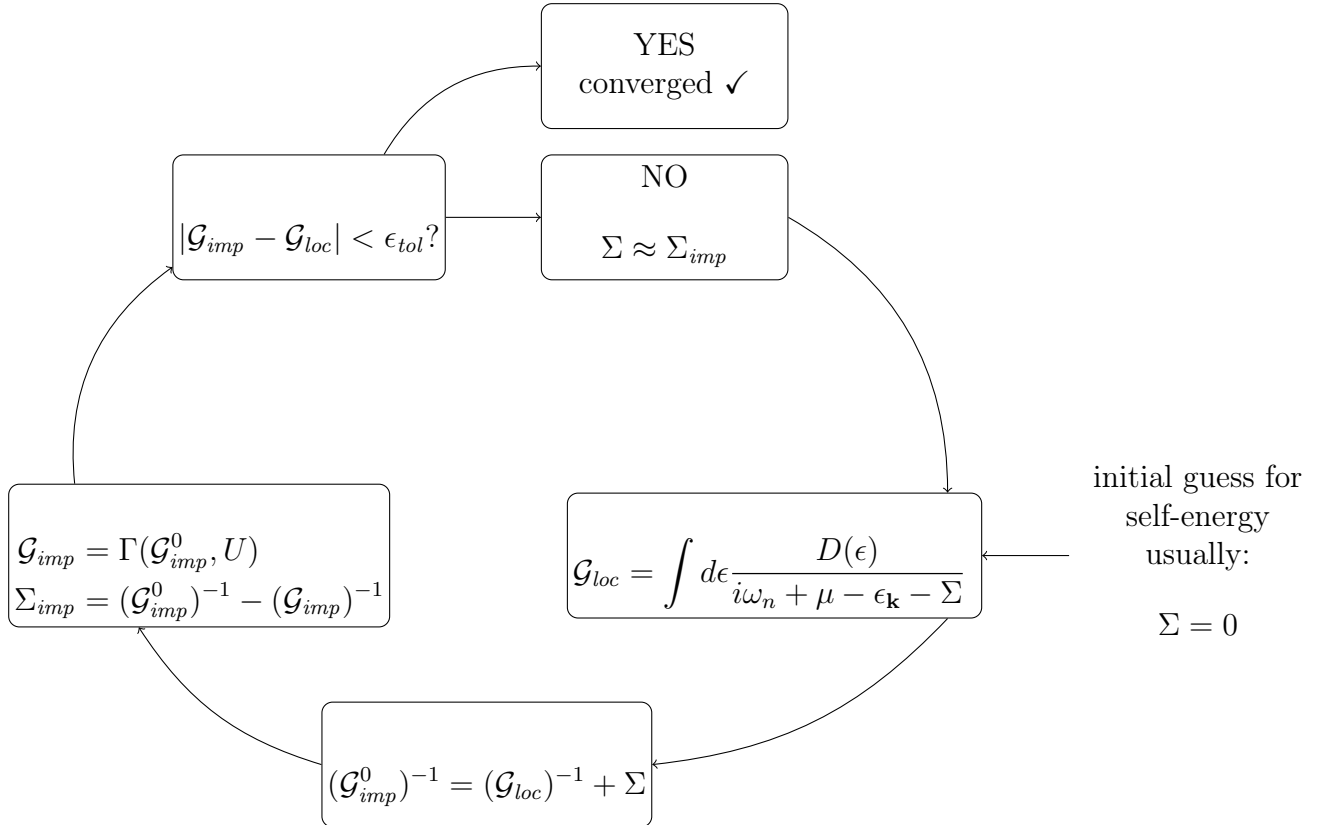
Figure 1.8: self consistency loop of DMFT. All Green's functions and self-energies are given in Matsubara frequencies

1.4.2 The self-consistency loop for two impurities

Due to the bipartite form of the honeycomb lattice we need to consider two impurities, one at atom A and another at atom B, as soon as the lattice sites become different due to ordering. This leads to a slightly altered situation as shown in figure 1.9, where two loops, similar to the one of figure 1.8, are implemented to calculate the self-energies for the different Atoms separately and are brought together for the evaluation of $\mathcal{G}_{loc}$. $\mathcal{G}_{loc}$ is then given by a block-diagonal Green's function, containing one block for each

impurity. Equivalent to the above situation, convergence is reached when both

$$
\begin{aligned}
(\mathcal{G}_{loc})_A &\overset{!}{=} (\mathcal{G}_{imp})_A \\
(\mathcal{G}_{loc})_B &\overset{!}{=} (\mathcal{G}_{imp})_B .
\end{aligned}
\tag{1.84}
$$
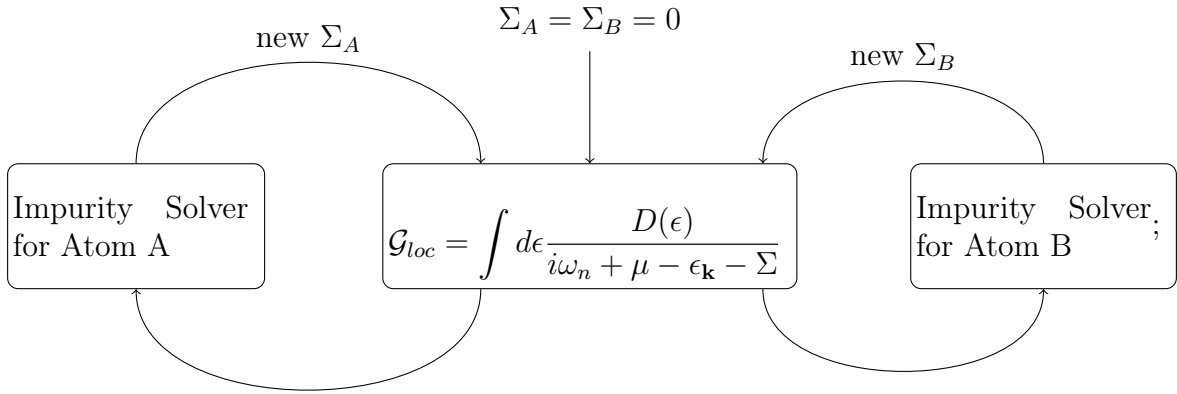
Figure 1.9: self consistency loop of DMFT considering 2 impurities, all Green's functions and self-energies in Matsubara frequencies

1.4.3 Calculation of the filling within DMFT

As we are interested in the determination of ordered phases a way to calculate particle densities from Green's functions is needed.

Therefore, we take equation (1.70) and replace τ' with zero and τ with an infinitesimally small $-\delta$ ($\delta > 0$)

$$
\mathcal{G}_{loc}^{\sigma}(-\delta) = -\left\langle T c_{i,\sigma}(-\delta) c_{i,\sigma}^{\dagger}(0) \right\rangle = \left\langle c_{i,\sigma}^{\dagger}(0) c_{i,\sigma}(-\delta) \right\rangle
\tag{1.85}
$$

Taking the limit $\delta \to 0$ thus gives

$$
\lim_{\delta \to 0^+} \mathcal{G}_{loc}^{\sigma}(-\delta) = \lim_{\delta \to 0^+} \left\langle c_{i,\sigma}^{\dagger}(0) c_{i,\sigma}(-\delta) \right\rangle = \langle n_{i\sigma} \rangle
\tag{1.86}
$$

But $\mathcal{G}_{loc}^{\sigma}(\tau)$ is the Fourier transformed of $\mathcal{G}_{loc}^{\sigma}(i\omega_n)$,

$$\langle n_{i\sigma}\rangle_{loc} = \lim_{\delta \to 0^+} \frac{1}{\beta} \sum_{\omega_n} e^{i\omega_n \delta} \mathcal{G}_{loc}^{\sigma}(i\omega_n). \tag{1.87}$$

This means that there is a direct connection between the Matsubara Green's function for a given sublattice o and the average particle density on this sublattice. But this must be true for both the impurity and the local Green's function. Hence the convergence criterion for our purpose implies that

$$\left| \langle n_{o\sigma}\rangle_{loc} - \langle n_{o\sigma}\rangle_{imp} \right| < \epsilon_{tol}$$
$$\left| \left(\langle n_{o\sigma}\rangle_{imp} \right)_i - \left(\langle n_{o\sigma}\rangle_{imp} \right)_{i+1} \right| < \epsilon_{tol} \tag{1.88}$$
$$\left| (\langle n_{o\sigma}\rangle_{loc})_i - (\langle n_{o\sigma}\rangle_{loc})_{i+1} \right| < \epsilon_{tol}$$

must be fulfilled for the individual spin classes $\uparrow$ and $\downarrow$ of both sublattices A and B separately.

1.4.4 Exact limits

There are three limits in which the DMFT approximation becomes exact:

1. In the **non-interacting limit**, i.e., $U = 0$. Taking the interaction strength to zero makes $\Sigma = 0$ and hence $\mathcal{G}$ equal to $\mathcal{G}^0$. The local Green's function is therefore reduced to the free on-site Green's function. As the self-energy is not just **k**-independent but even zero, the approximation becomes exact.

2. In the **atomic limit**. When the hopping amplitude t_{ij} vanishes (isolated Atoms) also $\epsilon_{\mathbf{k}}$ must vanish. Equation (1.80) implies then that $\Delta(i\omega_n) = 0$, i.e. the bath is completely decoupled and Σ can only have on-site components.

3. In the **limit of infinite coordination**, similar to MFT. As shown by Metzner and Vollhardt [9] the self-energy becomes a local quantity in the limit of infinite dimensions.

1.4.5 Solving the AIM - (CT-QMC)

To solve the Anderson impurity model a variety of methods, such as iterative perturbation theory (ITP), numerical renormalization group (NRG), exact diagonalisation (ED), quantum Monte-Carlo (QMC, CT-QMC) and equation of motion based methods (EO) exist. As the method used here is based on quantum-Monte-Carlo we will limit the discussion on this.

Simulations based on the Hirsch-Fye algorithm [10] have been for almost 20 years the method of choice. However, Hirsch-Fye QMC requires an equally spaced discretisation of imaginary time, which turns out to be a huge drawback in case of low temperatures and/or strong interactions. Therefore continous-time approaches (CT-QMC), which do not require time discretisation, have become increasingly important.

The principle of CT-QMC algorithms is a diagrammatic expansion of the partition function. Hereby the Hamiltonian (1.71) is split into two parts

$$H = H_a + H_b \tag{1.89}$$

which gives a partition function with respect to H_a expanded in powers of H_b, which does not need to be discretised in the termodynamical time interval $0 \leq \tau \leq \beta$,

$$
\begin{aligned}
Z =& Tr\left[Te^{-\beta H_a}\exp\left[-\int_0^\beta d\tau H_b(\tau)\right]\right] \\
=& \sum_k (-1)^k \frac{1}{k!}\int_0^\beta d\tau_1 \cdots \int_{\tau_{k-1}}^\beta d\tau_k Tr\left[Te^{-\beta H_a}H_b(\tau_k)H_b(\tau_{k-1})\cdots H_b(\tau_1)\right]
\end{aligned}
\tag{1.90}
$$

The trace can now be represented by Monte-Carlo methods, sampling stochastically over all $\tau...\tau_k$ and all orders of pertubation k.

As the method does not require a separation into an 'interacting' and a 'non-interacting' term multiple kinds of expansions are possible. The most common ones are the strong-coupling expansion in terms of $H_{coupling}$ and the weak-coupling expansion in powers of the interaction-term H_{atom}. In this work the strong-coupling approach [11] was used. For a more detailed overview on the different CT-QMC Methods the reader is referred to [12].

1.4.6   Results

For all calculations in this section the following parameters where chosen:

- 400 **k**-points in the Brillouin zone (just like in MFT).

- An inverse temperature of $\beta t = 40$.

- A tolerance of $\epsilon_{tol} \geq 10^{-2}$.

- A mixing of Σ between 1.0 and 0.8.

In order to perform DMFT calculations the TRIQS library was used [13].

Only on-site interaction (SDW-transition)

As we already expect SDW ordering for strong on-site interactions (see MFT-results and the considerations for a linear atomic string), we may just implement one of the two self-consistency loops (e.g. for sublattice A) drawn in figure 1.9 and use for the quantities of the second (e.g. sublattice B) the according anti-symmetric solutions

$$
\begin{aligned}
\Sigma_{B\uparrow} = \Sigma_{A\downarrow} \quad & \mathcal{G}_{imp}^{B\uparrow} = \mathcal{G}_{imp}^{A\downarrow} \\
\Sigma_{B\downarrow} = \Sigma_{A\uparrow} \quad & \mathcal{G}_{imp}^{B\downarrow} = \mathcal{G}_{imp}^{A\uparrow}.
\end{aligned}
\tag{1.91}
$$

Similar to the splitting in the particle densities within MFT, in DMFT we use a finite splitting in the initialization of the self-energy to obtain ordered phases, i.e.,

$$
\begin{aligned}
\Sigma_{A,\uparrow} &= c \\
\Sigma_{A,\downarrow} &= -c
\end{aligned}
\tag{1.92}
$$

with c being a constant (we used values between 0.5 and 1.8).

Due to the effect of fluctuations DMFT should run into a magnetic solution (for high enough U) also without this approach, but taking an adequate splitting leads to a faster convergence.

As an example, impurity and lattice Green's functions in Matsubara frequency space calculated with on-site interaction of $U = 4t$ are plotted in figure 1.10. We can clearly see that they are coinciding, and the DMFT SC condition is fulfilled.

To illustrate the convergence of the filling of the different orbitals, the evolution of the densities throughout the iterations is plotted in figure 1.11 (this is similar to MFT).
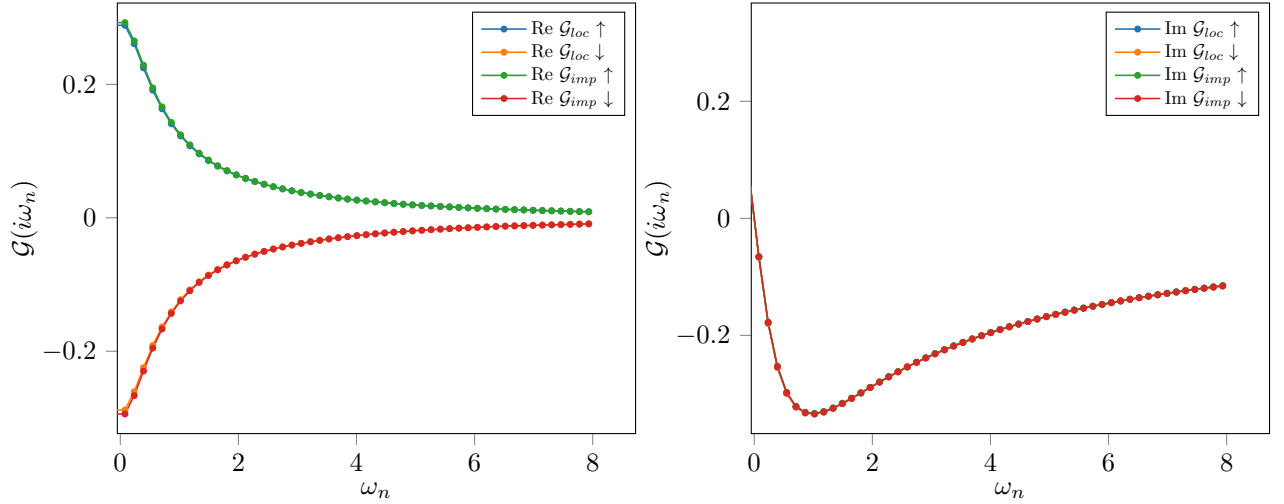
Figure 1.10: Convergence criteria for DMFT: comparison of $\mathcal{G}_{imp}\left(i\omega_n\right)$ and $\mathcal{G}_{loc}\left(i\omega_n\right)$ for the last iteration using $U = 4t$.
left: real part, right: imaginary part. All quantities are given for one sublattice
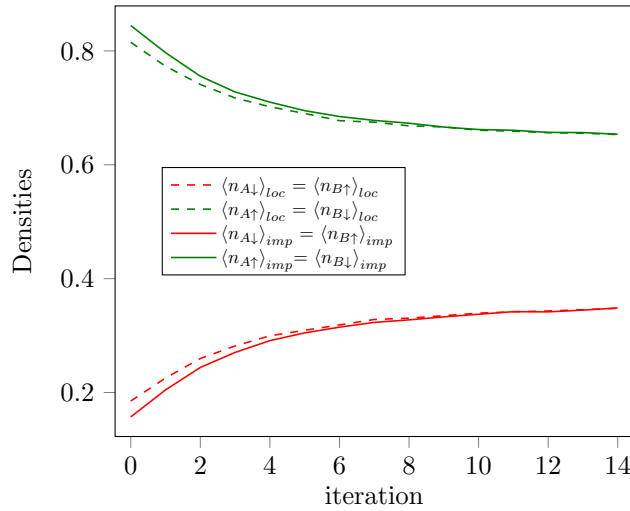
Figure 1.11: Evolution of the densities calculated from $\mathcal{G}_{loc}$ and $\mathcal{G}_{imp}$ over the iterations, $U = 4t$.

We performed calculations for several values of U and found a transition around $U_c \approx 3.5t$, which is a bit smaller than the similar dynamical cluster approximation result $U_c \lesssim 3.6t$ in [14].

The reason why MFT gives a much smaller result ($U_c = 2.23t$) is that fluctuations destroys ordering, i.e., in DMFT a stronger interaction is needed to observe a transition.

The SDW-transition for DMFT using purely on-site interaction is found in figure 1.12. To get a comparison, the MFT-result was plotted in the same figure.
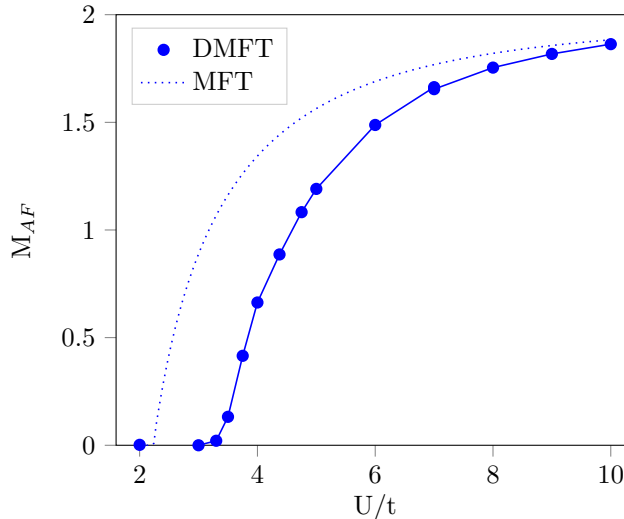
Figure 1.12: Phase transition using DMFT for V = 0

Only nearest-neighbor interaction (CDW-transition)

To get a CDW solution we no longer can symmetrize the impurity solutions like in equation (1.91), but need two independent impurity solvers for atom A and atom B. But as it is only possible in DMFT to include on-site interactions exactly, the nearest-neighbor interaction terms must again be approximated in a mean-field way. As $U = 0$ this gives

$$H_A = V n_A \langle n_B \rangle \quad H_B = V n_B \langle n_A \rangle, \tag{1.93}$$

where $\langle n_B \rangle$ and $\langle n_A \rangle$ need to be updated every iteration, starting with a inital splitting of $\langle n_B \rangle = 1 - c$ and $\langle n_B \rangle = 1 + c$ with c $\in [0, 1]$.

This, however, results in an effective non-interacting problem, and we should obtain the same result as for MFT. Nevertheless, since we use the strong coupling expansion CTQMC algorithm, this is a non-trivial test for the method.

Our (confirming) result is given in figure 1.13.
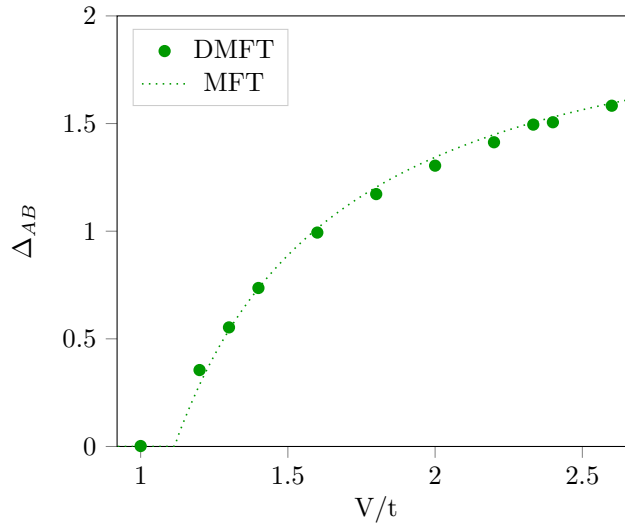
Figure 1.13: Phase transition using DMFT for U = 0

Interplay between the different phases

By including both local and nearest-neighbor interactions the phase diagram plotted in figure 1.14 was obtained. Solid lines represent the separation of the according phases within DMFT, whereas dotted lines give a comparison to MFT.

Just as in MFT, the critical U for the transition between the metallic and the SDW-phase has no dependence on V. Moreover, the separating line between metallic (M) and CDW-phase is an extension of the corresponding one obtained by mean-field calculations. Both of these results seem quite intuitive as the nearest-neighbor contribution remains in a mean-field approximation.

For the transition line between SDW and CDW we should stress the fact that the associated phase transition is of first order, and an calculation of the energy would be required to precisely determine the transition point. However, this is quite complicated within DMFT and was not performed -in. Instead, a large splitting in both the charge-ordering as well as the spin-ordering was chosen to initialize the calculations, arguing that DMFT runs into the solution associated with a steeper gradient. No solution with both SDW and CDW was found.

We find this line to differ from the mean-field solution, giving $V = U$. Aichhorn et al. [15] showed using variational cluster pertubation theory on a two dimensional square lattice, i.e., coordination number of $z = 4$) that SDW and CDW are seperated by the line of $U = V$, confirming also earlier quantum monte-carlo studies. Apart from the

fact that the position of the transition in our case is not unquestionable, we think that the deviation from $V = U$ might happen as a result of the different treatments of on-site and nearest neighbor interactions.
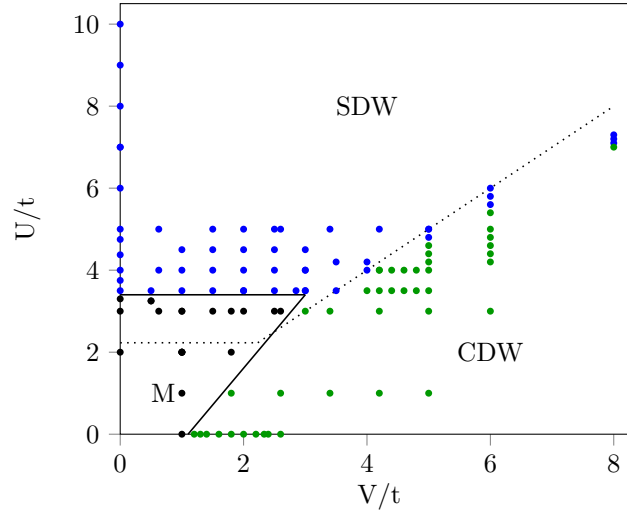
Figure 1.14: Phase diagram comparing MFT and DMFT. All points refer to self-consistent solutions received by DMFT-calculations. Black points signify that no finite order parameter was found (metallic-phase), green points denote a finite Δ_{AB} (CDW-phase) and blue points denote a finite M_{AF} (SDW-phase). Solid lines mark the transitions between the phases for DMFT. Dotted lines give the corresponding transitions obtained in MFT (figure 1.6).

Chapter 2

Relativistic treatment

2.1 Topological non-trivial phases

In this section the background of topological insulators will be shortly explained. This introduction is loosely based on [16].

2.1.1 From the Hall effect to the quantum spin Hall effect

If an electric field is applied to a metallic sample in longitudinal direction, and a magnetic field perpendicular to it, one can observe the so called **Hall effect**. The accelerated charges will get deflected (perpendicular to the plane spanned by magnetic and electric field) and separated by the resulting Lorentz force. The following accumulation at the boundaries gives a potential difference V_H and one can define the hall resistance as

$$R_H = \frac{V_H}{I}\frac{B}{q\rho_e},\tag{2.1}$$

with the current in the direction of the magnetic field I, the charge of the particles q and the density of the charge carriers ρ_e. The **anomalous Hall effect**, a similar effect, can be observed in ferromagnetic metals, even without an external magnetic field, leading to the empirical relation

$$R_H = R_0 B + R_A M,\tag{2.2}$$

where we find not just a proportionality to B, but also a contribution from the magnetization M. As the second part of the resistance R_A can not be explained simply by Lorentz force, it took almost 100 years to understand its physical origin.

Now we can link the AHE to the relativistic effect of spin-orbit coupling. Spin-orbit coupling can be understood as a momentum-dependent magnetic field coupling to the spin of the electron. Therefore in the presence of strong spin-orbit coupling, charged particles propagating in the same direction get separated according to their spin. As in ferromagnets the ratio between spin-up electrons and spin-down electrons is imbalanced, this results in an effective charge separation and therefore in the anomalous Hall effect.

But even without magnetic field or magnetization, the spin-dependent deflections can lead to an observable effect [17], the so called **spin Hall effect**. It consists of spin accumulation on the lateral surfaces of a current-carrying sample, the signs of the spin orientations being opposite on two opposite boundaries. Reversing the current direction leads to a reversion of the spin orientations.

Quantum Hall effect

In 1980 it was observed that in two-dimensional electron gases at semiconductor heterojunctions high magnetic fields in combination with sufficiently low temperatures lead to a quantized Hall conductance

$$\sigma_{xy} = \nu \frac{e^2}{h}, \tag{2.3}$$

with h being Planck's constant, the electron charge e and an integer ν. Additionally, the longitudinal resistance drops to zero repeatedly while increasing the magnetic field. This is explained by the Landau quantization of motion perpendicular to the magnetic field. The movement of a charged particle in a uniform magnetic field is given by a harmonic oscillator with the well known energy quantization

$$E_n = \hbar \omega_c \left(n + \frac{1}{2} \right) \tag{2.4}$$

and the cyclotron frequency $\omega_c = \frac{eB}{m}$.

The density of states is given by broadened delta-functions, where the spacing between the levels is proportional to B, while the broadening of the delta-functions depends on the temperature. This explain why the effect is only observed for low temperatures and strong magnetic fields. The Landau levels for a specific magnetic field and the behavior of the longitudinal as well as the Hall resistance $\rho_{xy} = 1/\sigma_{xy}$ with respect to magnetic field is shown in figure 2.1. Increasing the magnetic field continually lets Landau levels
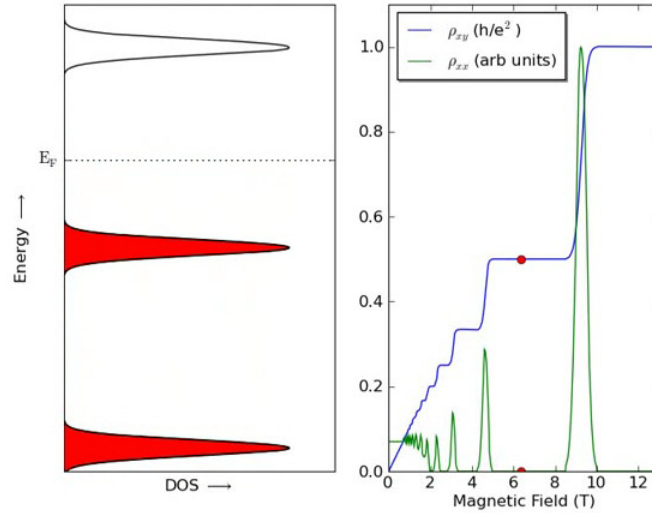
Figure 2.1: Hall resistance ρ_{xy} and longitudinal resistance ρ_{xx} with respect to the applied magnetic field are shown in the right figure. The corresponding Landau quantization for the magnetic field, indicated by the red point, is shown in the left figure. The position of the Fermi energy E_F shows that the bulk is insulating, but the vanishing resistance ρ_{xx} indicates conducting edge states. (adopted from [19])

pass through the Fermi energy.

Usually an insulator is defined as a material with a large band gap, i.e., there are no possible states close to the Fermi energy, whereas in a metal there are. In the case of the QHE, the longitudinal resistance however drops, exactly when the Fermi energy is between two Landau leves. In a semiclassic explanation, one can now find the charged particles in the bulk cycle around the magnetic flux (insulating), but in contrast, the particles on the boundary are not able to form a whole orbit, as they are confined by the edge. Therefore they start bouncing back and skip forward along the boundary forming a conduction channel. As the energy of the particles in the bulk is much lower than the energy of the electrons on the edge, there are no allowed states to scatter into other then the conduction channel itself. These so-called edge states are therefore insensitive to impuritiy scattering. The integer[1] ν in (2.3) is known as the filling factor giving the number of filled Landau levels and further also the number of edge states. It is now also realized that ν is a topological invariant (Chern-number).

---

[1]For completeness we should stress the fact, that this is just true for the integer quantum Hall effect, but that there is also something like the fractional quantum Hall effect where ν becomes a rational fraction (first observed in 1982 [18])

Quantum Spin Hall Effect

In 1987 Haldane [20] showed (for a honeycomb-lattice model) that breaking time-reversal symmetry can lead to a quantum Hall effect even in the absence of magnetic field or Landau levels. This quantum generalization of the anomalous Hall effect QAHE has been experimentally shown in 2013 [21].

Following Haldane, Kane and Mele created a model for a quantum generalization of the spin Hall effect by combining two quantum anomalous Hall effects of spin-up and spin-down electrons. The opposite chirality of spin-up and spin-down electrons results in two edge states traveling in opposite directions, which gives a vanishing charge current, but a non-zero spin current

$$\frac{\hbar}{2e} \left(\sigma_{xy}^{\uparrow} - \sigma_{xy}^{\downarrow} \right) = \frac{2}{4\pi}. \tag{2.5}$$

The generalization of this quantum spin Hall effect to other dimensions is called topological insulator. A topological insulator behaves like an insulator in the balk while as a metal on the boundary. However in this thesis we concentrate on the two dimensional honeycomb lattice, therefore in the following sections topological phase and quantum spin Hall phase will be used as synonyms. In figure 2.2 an overview of the different kinds of Hall effects is shown.
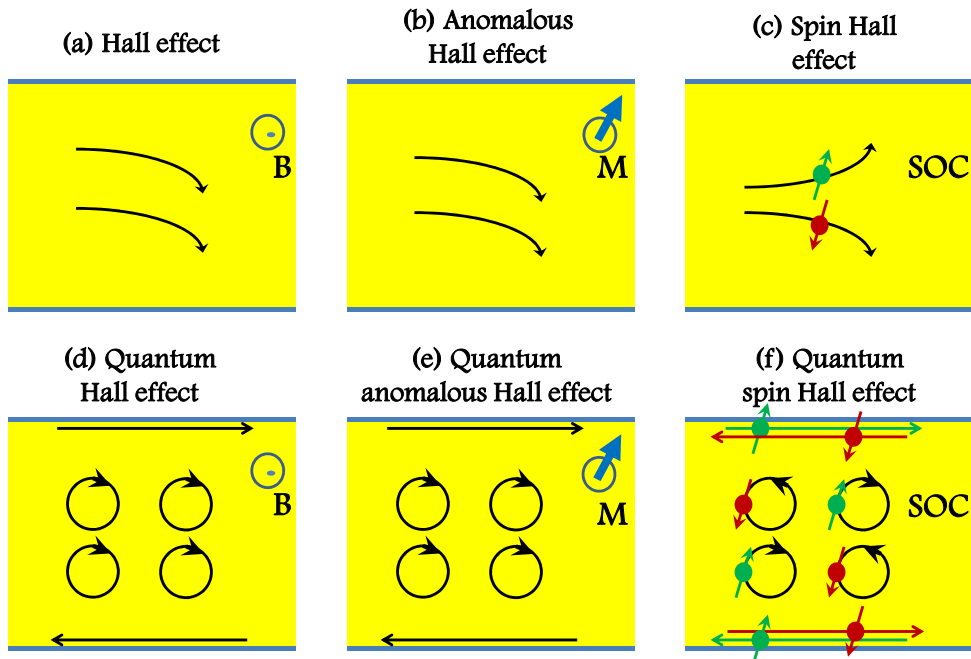
Figure 2.2: Overview on the different types of (quantum) Hall effects, B: magnetic field, M: magnetization, SOC: spin-orbit coupling (adopted from [22])

2.1.2 Berry phase and topological invariants

The choice of a Bloch state $|u_{n\mathbf{k}}\rangle$ (see Appendix A) is always defined just up to a phase. The transition

$$|u_{n\mathbf{k}}\rangle \rightarrow e^{if(\mathbf{k})} |u_{n\mathbf{k}}\rangle \tag{2.6}$$

has no observable effect.

When we consider a system Hamiltonian $H(\mathbf{R})$ adiabatically evolving in time through a parameter $\mathbf{R} \rightarrow \mathbf{R}(t)$ on a closed path, the time evolved state $|\phi_n(t)\rangle$ is related to its instantaneous eigenfunction $|u_n(\mathbf{R}(t))\rangle$ in the following way

$$|\phi_n(t)\rangle = e^{i\gamma_n(t)} e^{-\frac{i}{\hbar} \int_t^0 dt' \epsilon_n(\mathbf{R}(t'))} |u_n(\mathbf{R}(t))\rangle, \tag{2.7}$$

with a dynamical phase (second exponential) and a global phase γ_n which depends just on the path and cannot simply be transformed away by a gauge transformation.

For a closed path γ_n is given by

$$\gamma_n = i \oint_C d\mathbf{R} \langle u_n(\mathbf{R}) |\nabla_{\mathbf{R}}| u_n(\mathbf{R})\rangle \tag{2.8}$$

and is known as the Berry phase, which can, due to the single-valued condition of the wave function, just take values of $2\pi n$ (n being an integer).

This Berry-phase is connected to the Chern topological invariant in a two dimensional topological insulators

$$C = \sum_n \oint_{\partial Bz} \frac{d\mathbf{k}}{2\pi} \cdot i \langle u_n(\mathbf{k}) |\nabla_{\mathbf{k}}| u_n(\mathbf{k})\rangle, \tag{2.9}$$

which is a uniquely defined integer as long as the gap between valance and conduction band remains finite. It is equal to ν of the (integer) quantum hall effect (equation (2.3). For the spin Hall effect C will vanish (as time-reversal symmetry is preserved), however as long as spin is conserved, a spin chern number may be defined by calculating the individual C^σ for each spin separately

$$C^s = \sum_\sigma \sigma C^\sigma = \frac{(C^\uparrow - C^\downarrow)}{2}. \tag{2.10}$$

The topological invariant classifying the quantum spin Hall effect is a so called $\mathbb{Z}_2$ invariant

$$\nu = C^s \mod 2, \tag{2.11}$$

taking two possible values, 0 for topologically trivial and 1 for non-trivial phases.
Even though in the absence of S_z-conservation the quantization of spin Hall conductance breaks down, the $\mathbb{Z}_2$ invariant can still be defined differently ([4]) and may lead to a nonzero result as long as time-reversal symmetry remains valid.

Protected topology

The spin Chern number C^s is protected by spin conservation, whereas the $\mathbb{Z}_2$ topological invariant is protected by time reversal symmetry. This means that as long as one of these conditions are present, the gap needs to close to change topology.

2.2 Spin-orbit coupling in Graphene

This term used here was derived by Kane and Mele [3, 4] following the work of Haldane [20]. Hereby σ^z gives the Pauli matrix in z-direction and ν_{ij} specifies whether the electron makes a right turn $(= +1)$ or a left turn $(= -1)$. An illustration of the ν_{ij} can be found in figure 2.3. The Hamiltonian can be written as

$$H_{SO} = i\lambda_{SO} \sum_{\langle\langle ij \rangle\rangle} \nu_{ij} c_{i\sigma}^\dagger \sigma^z c_{i\sigma}. \tag{2.12}$$
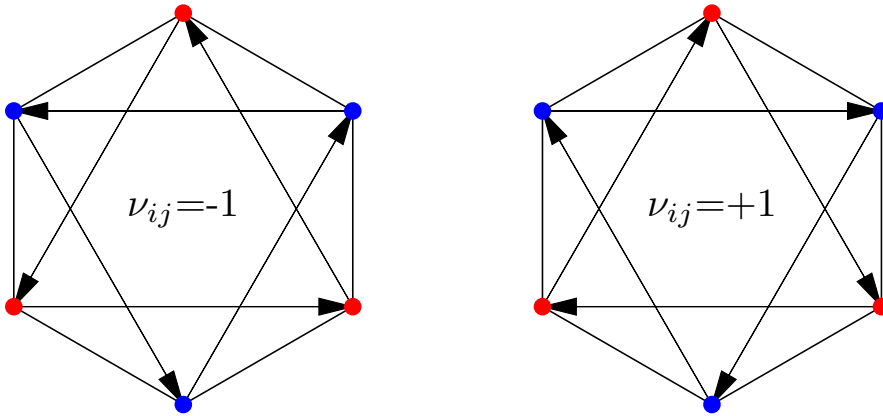
Figure 2.3: Illustration of the sign ν_{ij} for the honeycomb lattice. Every right turn gives ν_{ij} the value $+1$ and every left turn the value -1.

It has been shown by Zheng *et al.* [5] that this term also conserves particle hole symmetry. Hence, adding it to the extended Hubbard model leaves the chemical potential at $\mu = \frac{U}{2} + V$.

Including spin-orbit coupling to the extended Hubbard model finally leads to the complete model Hamiltonian this thesis is concentrated on:

$$H = -t \sum_{\langle ij \rangle, \sigma} c_{i\sigma}^\dagger c_{i\sigma} + U \sum_i n_{i\uparrow}^c n_{i\downarrow}^c + W \sum_{\langle ij \rangle} n_i^c n_j^c + i\lambda_{SO} \sum_{\langle\langle ij \rangle\rangle} \nu_{ij} c_{i\sigma}^\dagger \sigma^z c_{i\sigma} \tag{2.13}$$

The k-dependent Hamiltonian $H'(\mathbf{k})$ of equation (1.53) thus modifies as follows

$$H'(\mathbf{k}) = \begin{pmatrix} \gamma_{\mathbf{k}} & -g_{\mathbf{k}} & 0 & 0 \\ -g_{\mathbf{k}}* & -\gamma_{\mathbf{k}} & 0 & 0 \\ 0 & 0 & -\gamma_{\mathbf{k}} & -g_{\mathbf{k}} \\ 0 & 0 & -g_{\mathbf{k}}* & \gamma_{\mathbf{k}} \end{pmatrix} \qquad (2.14)$$

with

$$\gamma_{\mathbf{k}} = 2\lambda_{SO} \left[2\sin\left(\frac{a}{2}k_x\right)\cos\left(\frac{a}{2}\sqrt{3}k_y\right) - \sin\left(ak_x\right) \right]. \qquad (2.15)$$

As spin-orbit coupling breaks the degeneracy of spin-up and spin-down and couples the spin to the orbital moment, one loses SU(2) symmetry in the spin sector. This means that in-plane (xy) magnetization will generally be energetically different from out-of plane (z) magnetization. In MFT spin-directions are decoupled, therefore we will always run into the local minimum of the considered orientation, but also within DMFT we know from experience that we cannot flip the magnetic orientation within a regular DMFT-loop. Therefore in the following both directions are discussed.

Even though it is already known that the minimum in energy will be found for an purely in-plane magnetic order [23, 24], for completeness we will first concentrate on the solution for a magnetic order in z-direction.

2.3   Out-of plane direction

2.3.1   Results in MFT

In this case the total Hamiltonian (eq. (1.48)), becomes block-diagonal with two 2×2 spin-blocks, it can be diagonalized analytically and gives the following energy-bands:

$$
\begin{aligned}
E_{\uparrow\pm} &= \frac{U \langle n_\downarrow \rangle + V \langle n \rangle}{2} \pm \sqrt{|g_k|^2 + [\gamma_k - 0.5 \cdot (U(\langle n_{B\downarrow} \rangle - \langle n_{A\downarrow} \rangle) - V\Delta_{AB})]^2} \\
E_{\downarrow\pm} &= \frac{U \langle n_\uparrow \rangle + V \langle n \rangle}{2} \pm \sqrt{|g_k|^2 + [\gamma_k + 0.5 \cdot (U(\langle n_{B\uparrow} \rangle - \langle n_{A\uparrow} \rangle) - V\Delta_{AB})]^2}
\end{aligned}
\tag{2.16}
$$

We assume that no anti-ferromagnetic moment is present (which turns out to be generally true, if all parameters $\langle n_{i\sigma} \rangle$ are chosen arbitrarily and plugged into the self-consistent equation (1.59)) and first terms to be equal to the chemical potential (1.65)

$$
\begin{aligned}
E_{\uparrow\pm} &= \mu \pm \sqrt{|g_k|^2 + [\gamma_k - 0.5 \cdot (U(\langle n_{B\downarrow} \rangle - \langle n_{A\downarrow} \rangle) + V\Delta_{AB})]^2} \\
E_{\downarrow\pm} &= \mu \pm \sqrt{|g_k|^2 + [\gamma_k + 0.5 \cdot (U(\langle n_{B\uparrow} \rangle - \langle n_{A\uparrow} \rangle) + V\Delta_{AB})]^2}.
\end{aligned}
\tag{2.17}
$$

Effect of spin-orbit coupling on the band-structure ($V = U = 0$)

Setting the spin-orbit coupling λ_{SO} to a finite value results in an opening of the gap, see figure 2.4. This is similar to the situation of a transition to an ordered state. However, unlike the gap-opening associated with an order parameter where the bands are continuously dragged apart when one increases U (or V, resp.), for a SO-coupling induced gap opening the energy at the symmetry points M and M' remains unaffected and hence above a critical value of λ_{SO} the gap remains constant.
Plugging K/K' and M/M' into equation (2.17) ($U = V = 0$) gives

$$
\begin{aligned}
\Delta_{\mathbf{K}} = \Delta_{\mathbf{K}'} &= 6\sqrt{3}\lambda_{SO} \\
\Delta_{\mathbf{M}} = \Delta_{\mathbf{M}'} &= 2t.
\end{aligned}
\tag{2.18}
$$

The gap is hence for $\lambda_{SO} < 1/(3\sqrt{3})t$ determined by $\Delta_{\mathbf{K}}$ and for $\lambda_{SO} > 1/(3\sqrt{3})t$ by $\Delta_{\mathbf{M}}$.
More importantly, the gap induced by SO-coupling implies a topologically non trivial phase. Using the python package Z2Pack [25, 26] to calculate ν this was confirmed.
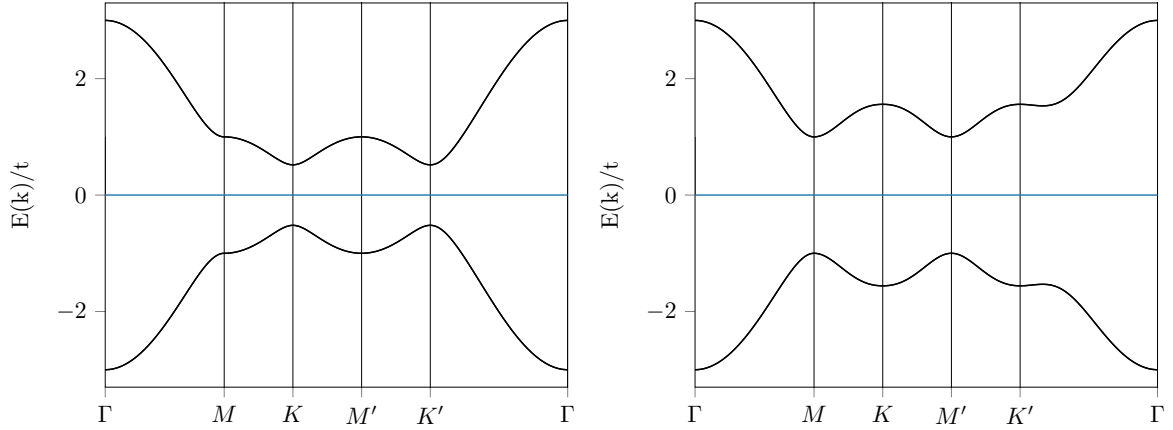
Figure 2.4: Dispersion relation for $\lambda_{SO} = 0.1$ (left) and $\lambda_{SO} = 0.3$, for $U = V = 0$

Spin-orbit coupling together with SDW ($V = 0$)

A finite λ_{SO} together with a non-vanishing SDW-order parameter M_{AF} destroys the degeneracy at the time reversal invariant **K** - points (figure 2.5 (right)), i.e., time reversal symmetry is broken. But as long as S^z is conserved we can use the definition of equation (2.11) to calculate ν.

The transition from semi metallic to SDW for $\lambda_{SO} = 0.3$ can be taken from figure 2.5 (left). As a gap closing may indicate, and is a necessary condition for, a topological phase transition, the gap is also plotted in the same figure. After checking ν before and after the gap closing we can distinguish three different phases

- quantum spin Hall state (QSH)

- quantum spin Hall state together with spin-ordering (SDW-QSH)

- topologically trivial SDW-phase (SDW)

separated by U_s^c (SDW-transition) and U_g^c (gap closing).
The according transitions for different values of λ_{SO} are plotted in figure 2.6.
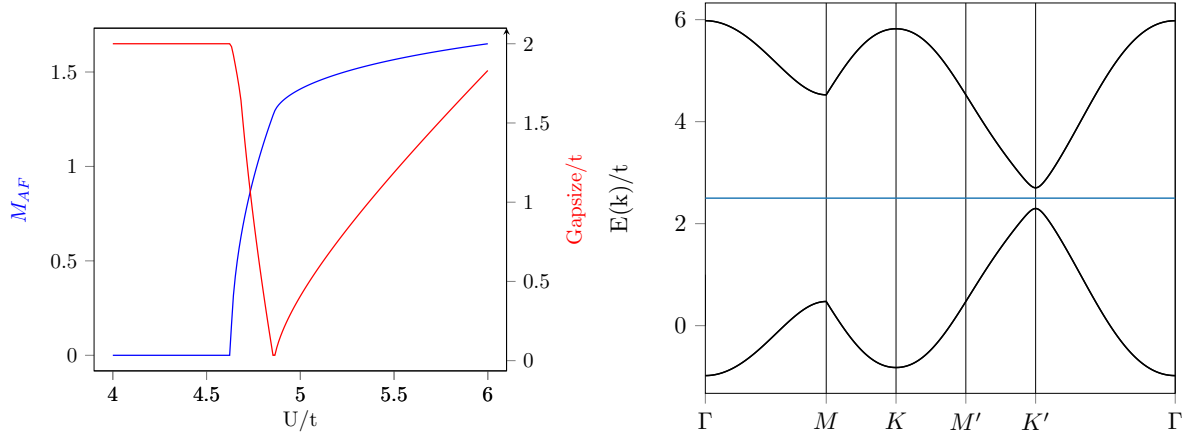
Figure 2.5: SDW-transition (left) and dispersion relation for $U = 5t$, $V = 0$ (right), $\lambda_{SO} = 0.3$
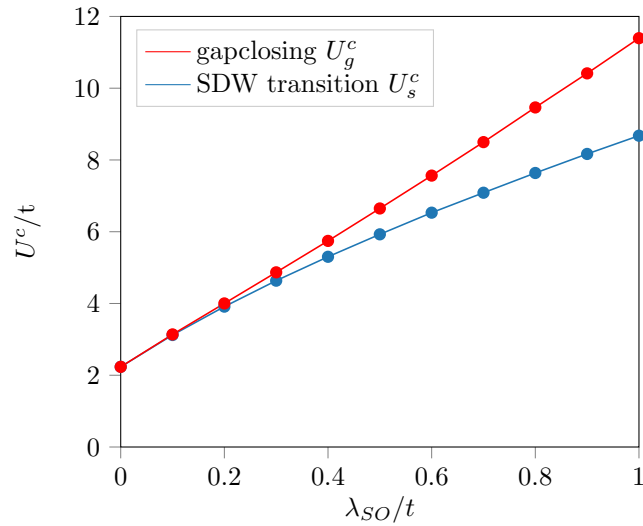
Figure 2.6: Critical values for the on-site interaction U for different λ_{SO} and $V = 0$

Spin-orbit coupling together with CDW ($U = 0$)

In the presence of SO-coupling and charge ordering the degeneracy of the spin sectors is broken. This is illustrated in figure 2.7 (right), where we can find two non-overlapping (except for M, M' and Γ) energy-bands below the chemical potential. This is caused by the broken inversion symmetry accompanying an energy difference between the sublattices. However, time-reversal symmetry is preserved as the dispersion at the respective points is the same.

Similarly to above, for the transition from QHS to CDW, a CDW-QSH phase in be-
tween the two critical values V_c^c and V_g^c can be found. For different values of λ_{SO} we
observe a very similar situation as above (figure 2.8).
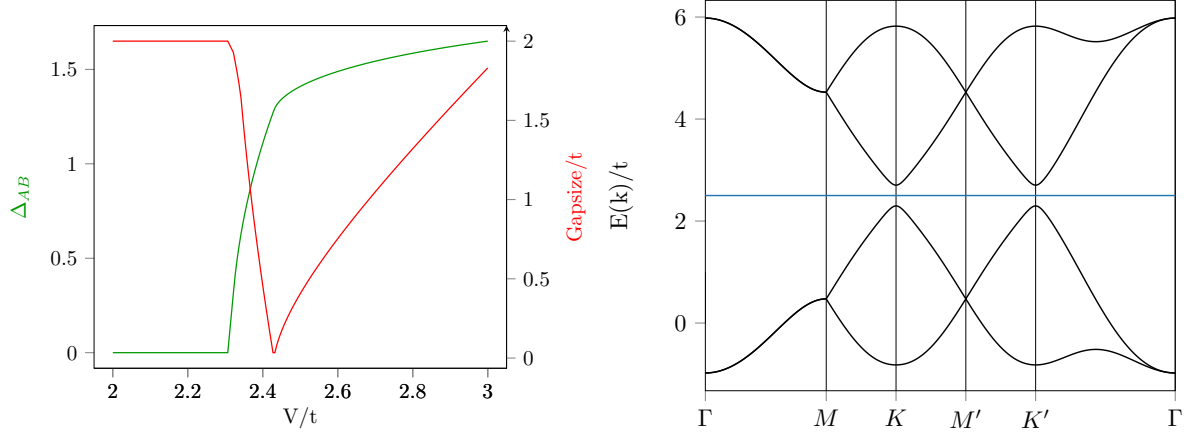
Figure 2.7: CDW-transition (left) and dispersion relation for $U = 0t$, $V = 2.5t$ (right),
$\lambda_{SO} = 0.3$
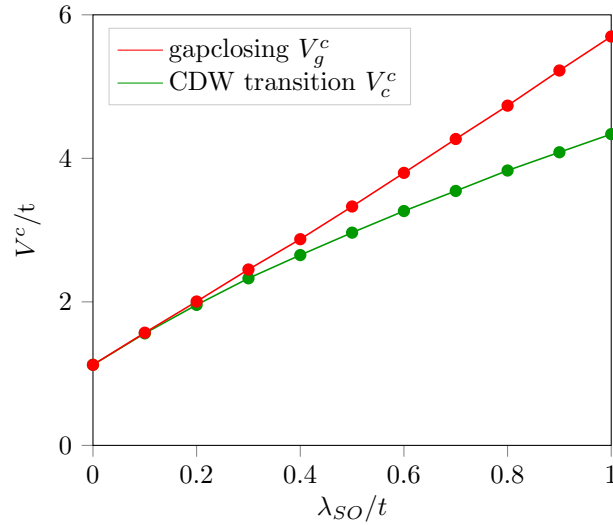
Figure 2.8: Critical values for the nearest-neighbor interaction V for different λ_{SO} and
$U = 0$

What is noticeable in figure 2.8 is, that for a given λ_{SO} the critical value for the phase-
transition to the SDW-phase is always double the critical value of the phase transition

to the CDW-phase, i.e.,

$$V_c^c(\lambda_{SO}, U = 0) = \frac{U_s^c(\lambda_{SO}, V = 0)}{2}. \tag{2.19}$$

This also holds for the critical value of the gap closing.

Interplay between the different phases

Investigating the rest of the phase-diagram by implementing a self-consistent loop and taking into account the 3 parameters λ_{SO}, U and V, we notice three more interesting things, when setting the spin-orbit coupling to an arbitrary value:

- We always, independently of the starting-parameters, obtain either a pure CDW, SDW or unordered (all $n_{i\sigma} \equiv 0.5$) solution, i.e., there are no stable mixed solutions of CDW and SDW.

- The critical interaction value U_c^s between the semi-metallic and the SDW phases **does not depend on V**.

$$U_c^s(\lambda_{SO}, V) \equiv U_c^s(\lambda_{SO}) \tag{2.20}$$

  Whereas V_c^c starts at $U_c^s/2$ and increases with $U/2$

$$V_c^c(\lambda_{SO}, U) = \frac{U_c^s(\lambda_{SO}) + U}{2} \tag{2.21}$$

- in a certain region around $U \approx V$ for $U > U_c^g(\lambda_{SO})$ and $V > V_c^g(\lambda_{SO}, U_c^g)$ one ends up with different solutions for different initial parameters, i.e., if we start with a CDW(SDW)-like distribution of the density the self-consistent loop will give a CDW(SDW) solution. This is linked to a first order transition.

To clarify the last two points we will take a closer look at the total energy of the system. Therefore we first rewrite the particle densities using the definition of M_{AF} and Δ_{AB} (see equation (1.66) and (1.67)).

$$\langle n_{A\uparrow} \rangle = \frac{1}{2} - \frac{M_{AF} + \Delta_{AB}}{4} \quad \langle n_{B\uparrow} \rangle = \frac{1}{2} + \frac{M_{AF} + \Delta_{AB}}{4}$$
$$\langle n_{A\downarrow} \rangle = \frac{1}{2} + \frac{M_{AF} - \Delta_{AB}}{4} \quad \langle n_{B\downarrow} \rangle = \frac{1}{2} - \frac{M_{AF} - \Delta_{AB}}{4} \tag{2.22}$$

The total energy (1.57) thus is given by:

$$E_{tot} = -\frac{1}{N_\Lambda} \sum_{\mathbf{k}} \left(\sqrt{|g_k|^2 + \left[\gamma_k + 0.5 \cdot \left(\frac{U}{2}(M_{AF} - \Delta_{AB}) + V\Delta_{AB}\right)\right]^2} \right.$$
$$\left. + \sqrt{|g_k|^2 + \left[\gamma_k + 0.5 \cdot \left(\frac{U}{2}(M_{AF} + \Delta_{AB}) - V\Delta_{AB}\right)\right]^2} \right) \tag{2.23}$$
$$+ U\left(\frac{M_{AF}^2}{8} - \frac{\Delta_{AB}^2}{8}\right) + V\frac{\Delta_{AB}^2}{4} + c(U, V)$$

As we already know that in every self-consistent solution either M_{AF} or Δ_{AB} (or both) must be zero, we are interested in these cases.

Let us first just focus on the two different cases $V = 0$ and $U = 0$:

- $V = 0$ means that $\Delta_{AB} = 0$, too, which gives (see also [27])

$$E_{tot} = -\frac{2}{N_\Lambda} \sum_{\mathbf{k}} \sqrt{|g_k|^2 + \left[\gamma_k + \frac{U}{4}M_{AF}\right]^2} + U\frac{M_{AF}^2}{8} \tag{2.24}$$

- on the other hand $U = 0$ means $M_{AF} = 0$ and thus leads to

$$E_{tot} = -\frac{1}{N_\Lambda} \sum_{\mathbf{k}} \left(\sqrt{|g_k|^2 + \left[\gamma_{\mathbf{k}} + \frac{V}{2}\Delta_{AB}\right]^2} + \sqrt{|g_{\mathbf{k}}|^2 + \left[\gamma_{\mathbf{k}} - \frac{V}{2}\Delta_{AB}\right]^2} \right)$$
$$+ V\frac{\Delta_{AB}^2}{4} \tag{2.25}$$

Equation (2.24) and (2.25) have a very similar form, and if we choose $V = U/2$ and $M_{AF} = \Delta_{AB}$ they become almost equal, except that in equation (2.25) the two terms differ in there sign between $\gamma_{\mathbf{k}}$ and $\frac{V}{2}\Delta_{AB}$ and in (2.24) they don't. This corresponds to the degeneracy and non-degeneracy of the respective dispersion relationships in figure 2.7 and 2.5. However, if we take into account that $|g_{\mathbf{k}}|^2 \equiv |g_{-\mathbf{k}}|^2$ and $\gamma_{\mathbf{k}} \equiv -\gamma_{-\mathbf{k}}$ and

$\sum_{\mathbf{k}}$ goes over the whole brillouin zone the result for total energy will be the same. This explains why we are observing the exact same form of transition for V and U in respect to their ordering parameters they are associated with.

Lets further focus on the case where neither V nor U are zero. As either M_{AF} or Δ_{AB} must be zero to minimize the energy, we find in case of a SDW-solution for equation (2.23) no difference to the expression (2.24), which is consistent with the observation that the transition from SM to SDW is independent of V. On the other hand, in case of a CDW-solution ($M_{AF} = 0$), we can find that the total energy is given by

$$
E_{tot} = -\frac{1}{N_\Lambda} \sum_{\mathbf{k}} \left(\sqrt{|g_k|^2 + \left[\gamma_{\mathbf{k}} + \frac{1}{2} \left(V - \frac{U}{2} \right) \Delta_{AB} \right]^2} \right.
$$
$$
\left. + \sqrt{|g_{\mathbf{k}}|^2 + \left[\gamma_{\mathbf{k}} - \frac{1}{2} \left(V - \frac{U}{2} \right) \Delta_{AB} \right]^2} \right) + \left(V - \frac{U}{2} \right) \frac{\Delta_{AB}^2}{4}.
$$

$$(2.26)$$

Comparing (2.26) with (2.24), an effective V_{eff} in the form of

$$
V_{eff} = V - \frac{U}{2}
$$

$$(2.27)$$

is found.

This explains the U-dependence of V^c. On the other hand this means that for $V = U$ we have $V_{eff} = U/2$, which will give the same energy for the anti-ferromagnetic state and the charge-ordered-state for an equal value of the order-parameter. Therefore in the region where CDW and SDW are stationary solutions, $V = U$ gives the transition between those two phases.

The fact that in the direct neighborhood of $V = U$ always two stable solutions can be found indicates a phase-transition of first order.

To illustrate the two stationary solutions and to show that no other mixed solution (CDW+SDW) is possible, the total energy as a function of the order-parameters (2.23) is plotted in figure 2.9 for the two parameter sets ($U = 4$, $V = 4$, $\lambda_{SO} = 0.0$) and ($U = 4.3$, $V = 4$, $\lambda_{SO} = 0.0$) . The plot shows only values for $M_{AF} + \Delta_{AB} \leq 2$, as other combinations would require negative density values.

We can also find a saddle point between the two stationary CDW and SDW solutions. In the case of $U = V$ this point can be found on the line where $\Delta_{AB} = M_{AF}$. Using equation (2.22) this gives a random distribution over the two atoms for one spin-class

and an unequal distribution for the other spin-class. Initializing the self-consistency loop for $U = V = 5$ with that condition led to a metastable band structure shown in figure 2.10.
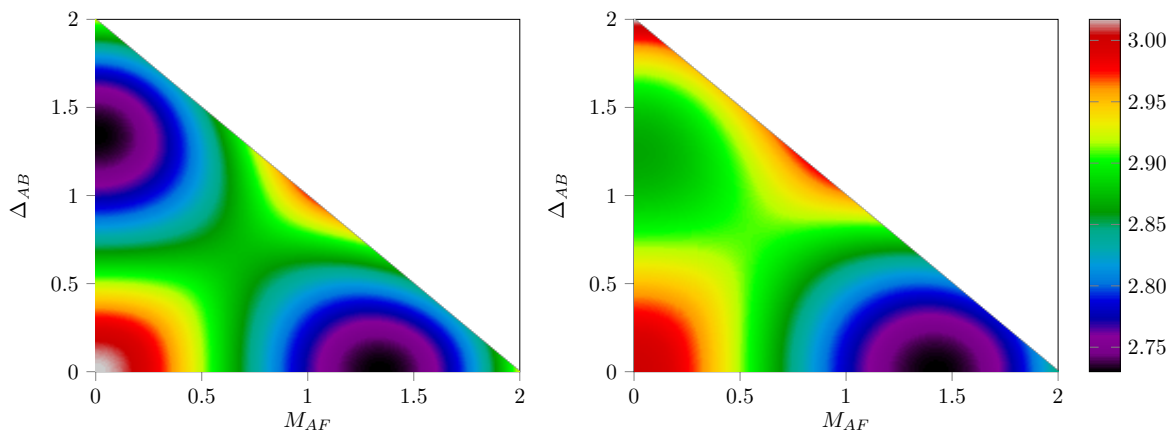
Figure 2.9: Total energy for $\lambda_{SO} = 0.0$ and V = 4,
left picture: U = 4, right picture U = 4.3
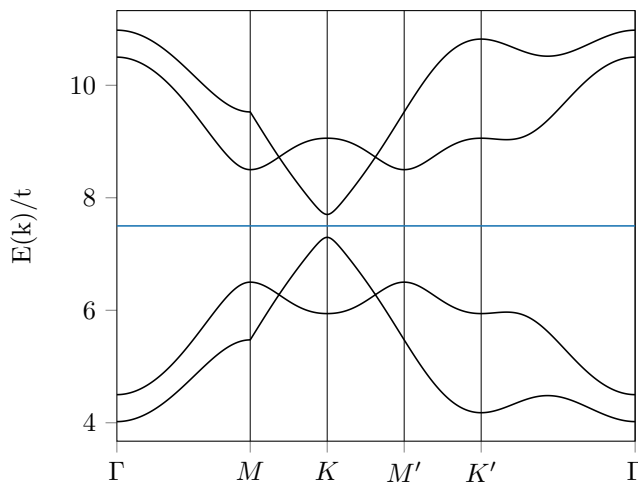
Figure 2.10: Band structure for $U = 5t$, $V = 5t$, $\lambda_{SO} = 0.3t$
(metastable solution: $M_{AF} = \Delta_{AB}$)

To conclude, our phase diagram for the extended Hubbard model for two values of λ_{SO} (0.5t and 0.9t) is shown in figure 2.11. For finite spin-orbit coupling the unordered phase becomes topologically non-trivial, and the in-between phase (CDW-QSH and SDW-QSH) appears which increases with increasing λ_{SO}. The phase diagrams can be

generated simply by the results shown in figure 2.6 and 2.8.
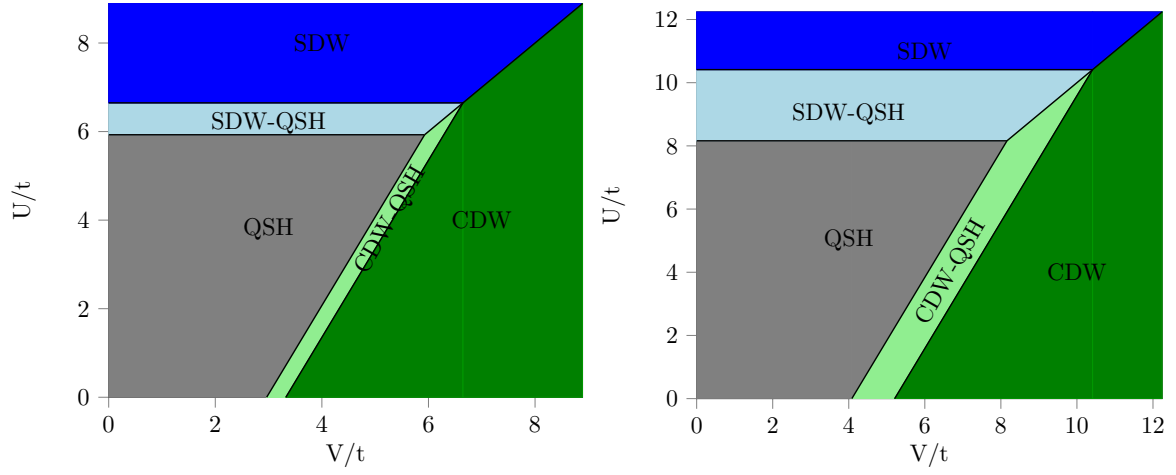
Figure 2.11: Phase diagrams for $\lambda_{SO} = 0.5t$ (left) and $\lambda_{SO} = 0.9t$ (right), with spin-ordering in z-direction

2.3.2 Results in DMFT

To recover an exact treatment of the on-site interaction, DMFT has again been applied to the problem and for $\lambda_{SO} = 0.2t$ and $V = 0$ a phase transition to SDW was calculated (see figure 2.12 (left)). The according critical value was found to be $U_c(\lambda_{SO} = 0.2) = 6.2(3)t$ and is indistinguishable from the topological transition, meaning that we could not find a QSH state with SDW order. Calculations with stronger spin-orbit couplings ($\lambda_{SO} = 0.4t$) turned out to demand too many warm up cycles and measurements within CTQMC, hence no other transitions of that kind are shown here.
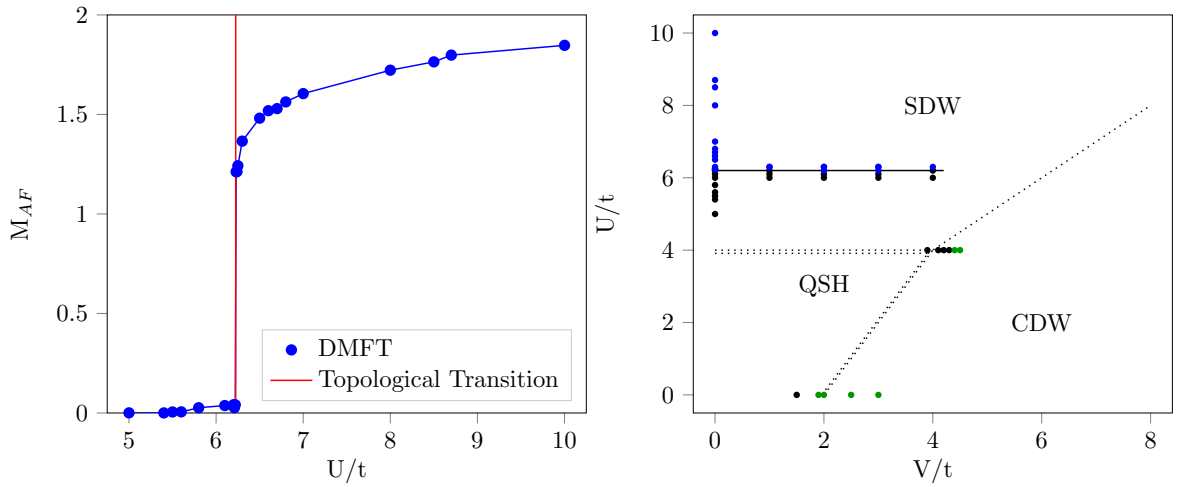
Figure 2.12: Phase transition for $V = 0$ (left). Phase diagram comparing MFT and DMFT for $\lambda_{SO} = 0.2t$ (right): All points refer to self-consistent solutions received by DMFT-calculations. Black points signify that no finite order parameter was found (metallic-phase), green points denote a finite Δ_{AB} (CDW-phase) and blue points denote a finite M_{AF} (SDW-phase). Solid lines mark the transitions between the phases for DMFT. Dotted lines give the corresponding transitions obtained in MFT

We calculated also different regimes of the phase diagram and plotted the results in figure 2.12 (right). Again U_c is found to be independent of the (MFT-treated) on-site interactions, and the transition line between QSH state and CDW state is roughly similar to mean field.

2.4   In-plane direction (in MFT)

Due to the symmetry of x- and y-direction, we can reduce our discussion to the x-direction.

To treat the extended Hubbard model including SO-coupling (2.13) within MFT (1.41) (1.42) for spin in the x-direction we replace the creation and annihilation operators in our model Hamiltonian as follows

$$
\begin{aligned}
c_{i\uparrow}^\dagger \to c_{i\to}^\dagger, & \quad c_{i\uparrow} \to c_{i\to} \\
c_{i\downarrow}^\dagger \to c_{i\leftarrow}^\dagger, & \quad c_{i\downarrow} \to c_{i\leftarrow}
\end{aligned}
\tag{2.28}
$$

Where $c_{i\to}^\dagger$ creates an electron with spin in the 'up' x-direction $(+x)$ and $c_{i\leftarrow}^\dagger$ creates an electron with spin in the 'down' x-direction $(-x)$ etc. But, this just has an effect on terms that explicitly depend on spin, like the U and the λ_{SO}-term.

We can find that H_U^x hence becomes diagonal in the x-basis of the spin, while H_{SO}^x is still diagonal in the z-basis. For the remaining terms these bases are equivalent. The total Hamiltonian hence, has no longer a block diagonal form and we cannot find a analytic expression similar to (2.17). To calculate the eigenenergies and eigenstates we evaluate the different terms in their eigenbasis and then transform one term into the other basis to diagonalize the full matrix.

H_U^x in the x-basis is given by

$$
(H_U^x)_x = \begin{pmatrix}
\langle n_A^\to \rangle & & & \\
& \langle n_B^\to \rangle & & \\
& & \langle n_A^\leftarrow \rangle & \\
& & & \langle n_B^\leftarrow \rangle
\end{pmatrix}
\tag{2.29}
$$

The rotation operator for rotations around the y axis by an arbitrary angle Θ states as follows:

$$
R_y(\Theta) = e^{-i\Theta\sigma_y} = \cos(\Theta/2)\cdot\begin{pmatrix} 1 & 0 \\ 0 & 1 \end{pmatrix} - i\sin(\Theta/2)\cdot\begin{pmatrix} 0 & -i \\ i & 0 \end{pmatrix} = \begin{pmatrix} \cos(\Theta/2) & -\sin(\Theta/2) \\ \sin(\Theta/2) & \cos(\Theta/2) \end{pmatrix}
\tag{2.30}
$$

As the transformation on lattice subspace must be the unitary matrix, the whole transformation from x- to the z-basis is given by:

$$T_{x \to z} = R_y(\pi/2) \circledast \mathbb{I} \tag{2.31}$$

The H_U^x Hamiltonian in z-basis therefore reads:

$$(H_U^x)_z = T_{x \to z} (H_U^x)_x T_{x \to z}^{-1}$$

$$= \cos^2(\Theta/2) \begin{pmatrix} \langle n_A^{\rightarrow} \rangle & & & \\ & \langle n_B^{\rightarrow} \rangle & & \\ & & \langle n_A^{\leftarrow} \rangle & \\ & & & \langle n_B^{\leftarrow} \rangle \end{pmatrix} + \sin^2(\Theta/2) \begin{pmatrix} \langle n_A^{\leftarrow} \rangle & & & \\ & \langle n_B^{\leftarrow} \rangle & & \\ & & \langle n_A^{\rightarrow} \rangle & \\ & & & \langle n_B^{\rightarrow} \rangle \end{pmatrix}$$

$$+ \sin(\Theta/2)\cos(\Theta/2) \begin{pmatrix} 0 & 0 & \langle n_A^{\leftarrow} \rangle - \langle n_A^{\rightarrow} \rangle & 0 \\ 0 & 0 & 0 & \langle n_B^{\leftarrow} \rangle - \langle n_B^{\rightarrow} \rangle \\ \langle n_A^{\leftarrow} \rangle - \langle n_A^{\rightarrow} \rangle & 0 & 0 & 0 \\ 0 & \langle n_B^{\leftarrow} \rangle - \langle n_B^{\rightarrow} \rangle & 0 & 0 \end{pmatrix}$$

$$\tag{2.32}$$

As one can see immediately, this transformation just gives a nontrivial result if there is a finite anti-ferromagnetic moment M_{AF} i.e. $\langle n_{i\sigma} \rangle \neq \langle n_{i\bar{\sigma}} \rangle$.

But for a change in the entire Hamiltonian one of the other terms also needs to transform nontrivial. If we perform the transformation now in the other direction ($T_{x \to z}^{-1} = T_{z \to x}$) for the H_{SO}^x term, we similarly obtain an expression which is non-trivially (if $\gamma_{\mathbf{k}}$ i.e. λ_{SO} is finite).

This means the spin-directions are degenerate if at least either λ_{SO} or M_{AF} is zero, thus we only experience a change to the out-of plane situation, when a finite anti-ferromagnetic moment is present. Therefore the transition from QSH to CDW will not change, but the U^c does. The observed values for different λ_{SO} are shown in figure 2.13. It is important to note here that there is gap closing neither at the SDW transition nor anywhere after. However, topology has changed and the critical value U_c for the topological transition is equal to the one for the SDW transition. That is caused by the fact that topology is no longer protected, as time-reversal symmetry is broken (due to a finite M_{AF}) and spin is no longer conserved (due to a finite λ_{SO}).
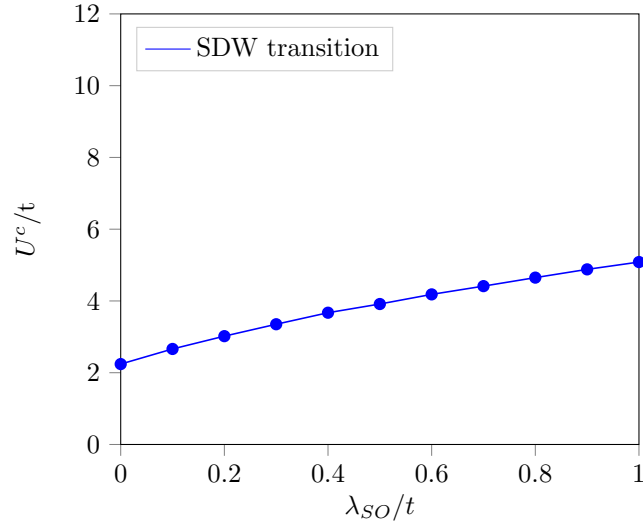
Figure 2.13: SDW transition as a function of λ_{SO} for $V = 0$ and for spin in xy-direction

A phase diagram for two different values of λ_{SO} is shown together with the according lines belonging to the out-of plane solutions in figure 2.14. Apart from the fact that the phase diagram is 'truncated' in favor of the SDW phase we observe a new transition between a topologically non-trivial CDW and the trivial SDW phase. Besides the condition of $V = U$ is fulfilled at least for strong interactions.
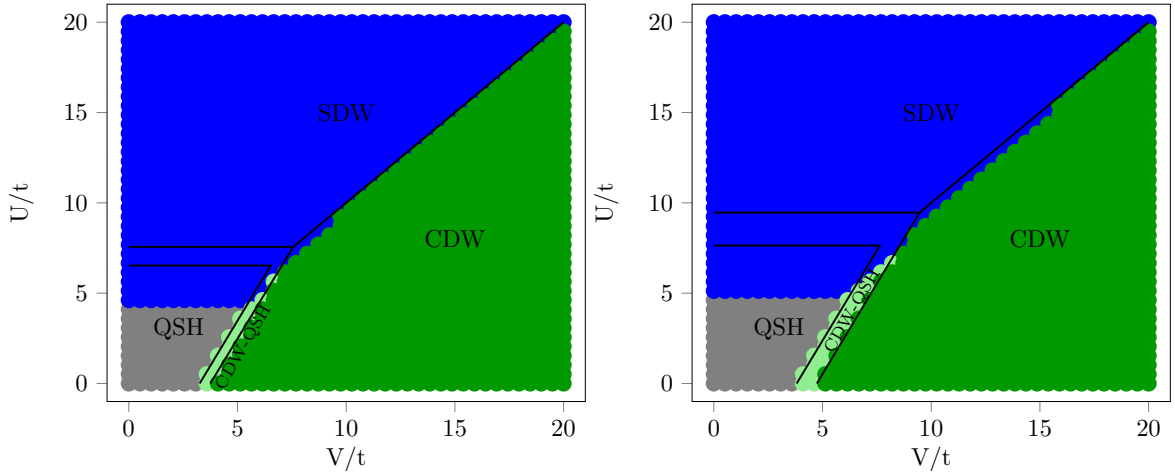
Figure 2.14: Phase diagram $\lambda_{SO} = 0.6$ (left), $\lambda_{SO} = 0.8$ (right). Solid lines are the according lines belonging to out-of plane orientation

Conclusion

In this work we investigated the general phase diagram of the extended Hubbard model on a honeycomb lattice, in particular with emphasis on the effects of spin-orbit coupling. Therefore we started using mean-field decoupling of both interaction terms and further recovered local fluctuations by means of DMFT to calculate the phase boundaries between metallic, topological, spin-density wave, and charge-density wave phases. In the first chapter the pure extended Hubbard model was studied and we found for the transition between metallic and SDW a critical on-site interaction of $U_{MFT}^c = 2.23t$ for MFT and $U_{DMFT}^c \approx 3.5t$ for DMFT. Both of which compare to values we found in the literature: $2.23t$ (MFT) and $\lesssim 3.6t$ (DCA which is similar to DMFT). Moreover we found that non-local interactions do not shift this value neither in MFT nor in DMFT, however for DMFT this might be intrinsic as nearest-neighbor interactions have still been treated in a mean-field approximation. In MFT for the transition between metallic and CDW phase, we found the simple conditions for the (effective) nearest-neighbor interaction of $V_{MFT}^c = (U_{MFT}^c + U)/2$ and in the case of very strong interactions, SDW and CDW are separated by a line fulfilling $V = U$. Both of these conditions have been shown analytically in the second chapter. The transition line between metallic and CDW remains in DMFT roughly at the same position. Even though $U \approx V$ should be a general condition, our calculations in DMFT have a stronger tendency towards SDW ordering. We considered the first-order type phase transition and/or the unequal treatment of on-site and nearest-neighbor interactions within our approximation to be the reason for that.

In the second chapter by adding spin-orbit coupling λ_{SO} we found four different phases in MFT, including QSH state, CDW, SDW and the mixed CDW-QSH. A SDW-QSH phase is just present in the metastable state of out-of plane magnetization. Qualitatively we find with increasing λ_{SO}, that the transition lines between the unordered (here QSH) and the ordered phases are shifted in favor of the unordered state and that the

in-between phase of CDW-QSH grows. In DMFT we calculated just the meta-stable state, as it can be treated more easily. We find for $\lambda_{SO} = 0.2t$ that the transition line between QSH and SDW is shifted to $U_{DMFT}^c \approx 6.2t$. An in-between phase of SDW-QSH cannot be found here.

Appendices

Appendix A

Bloch functions and Wannier functions

In a periodic lattice the wave function of an electron is given by a so called Bloch wave or Bloch state. The underlying Bloch theorem states that for a Hamiltonian of the form $H(\mathbf{r}) = H(\mathbf{r} + \mathbf{R})$ with the period of the crystal lattice $\mathbf{R}$ the eigenfunctions must have the form of

$$|\psi_{n,\mathbf{k}}(\mathbf{r})\rangle = e^{i\mathbf{k}\mathbf{r}} |u_{n,\mathbf{k}}(\mathbf{r})\rangle. \tag{A.1}$$

Where the cell periodic eigenstates $u_{n,\mathbf{k}}(\mathbf{r}) = u_{n,\mathbf{k}}(\mathbf{r} + \mathbf{R})$ together with the Bloch Hamiltonian $H(\mathbf{k}) = e^{-i\mathbf{k}\mathbf{r}} H(\mathbf{r}) e^{i\mathbf{k}\mathbf{r}}$ give the reduced Schrödinger equation

$$H(\mathbf{k}) |u_{n,\mathbf{k}}(\mathbf{r})\rangle = E_{n\mathbf{k}} |u_{n,\mathbf{k}}(\mathbf{r})\rangle \tag{A.2}$$

For (effectively) non-interacting systems, this gives the basis of band-structure calculations in a solids.

However function of that kind (equation (A.1)) do not allow spatial charge localizations, which is necessary for an accurate description of two-particle coulomb interactions. Therefore Wannier functions are introduced

$$\phi_{\mathbf{R}(\mathbf{r})} = \frac{1}{\sqrt{N}} \sum_{\mathbf{k}} e^{-i\mathbf{k}\mathbf{R}} \psi_{\mathbf{k}}(\mathbf{r}), \tag{A.3}$$

representing an orthogonal set of functions, similar to molecular orbitals, localized around each lattice site $\mathbf{R}$.

Bibliography

[1] P. R. Wallace. The Band Theory of Graphite. *Phys. Rev.*, 71:622–634, May 1947. doi: 10.1103/PhysRev.71.622. URL `https://link.aps.org/doi/10.1103/PhysRev.71.622`.

[2] K. S. Novoselov, A. K. Geim, S. V. Morozov, D. Jiang, Y. Zhang, S. V. Dubonos, I. V. Grigorieva, and A. A. Firsov. Electric Field Effect in Atomically Thin Carbon Films. *Science*, 306(5696):666–669, 2004. ISSN 0036-8075. doi: 10.1126/science.1102896. URL `http://science.sciencemag.org/content/306/5696/666`.

[3] C. L. Kane and E. J. Mele. Quantum Spin Hall Effect in Graphene. *Phys. Rev. Lett.*, 95:226801, Nov 2005. doi: 10.1103/PhysRevLett.95.226801. URL `https://link.aps.org/doi/10.1103/PhysRevLett.95.226801`.

[4] C. L. Kane and E. J. Mele. Z_2 Topological Order and the Quantum Spin Hall Effect. *Phys. Rev. Lett.*, 95:146802, Sep 2005. doi: 10.1103/PhysRevLett.95.146802. URL `https://link.aps.org/doi/10.1103/PhysRevLett.95.146802`.

[5] Dong Zheng, Guang-Ming Zhang, and Congjun Wu. Particle-hole symmetry and interaction effects in the Kane-Mele-Hubbard model. *Phys. Rev. B*, 84:205121, Nov 2011. doi: 10.1103/PhysRevB.84.205121. URL `https://link.aps.org/doi/10.1103/PhysRevB.84.205121`.

[6] S. Sorella and E. Tosatti. Semi-Metal-Insulator Transition of the Hubbard Model in the Honeycomb Lattice. *EPL (Europhysics Letters)*, 19(8):699, 1992. URL `http://stacks.iop.org/0295-5075/19/i=8/a=007`.

[7] Antoine Georges. Strongly Correlated Electron Materials: Dynamical Mean-Field Theory and Electronic Structure. 715, 03 2004.

[8] P. W. Anderson. Localized Magnetic States in Metals. *Phys. Rev.*, 124:41–53, Oct 1961. doi: 10.1103/PhysRev.124.41. URL `https://link.aps.org/doi/10.1103/PhysRev.124.41`.

[9] Walter Metzner and Dieter Vollhardt. Correlated Lattice Fermions in $d = \infty$ Dimensions. *Phys. Rev. Lett.*, 62:324–327, Jan 1989. doi: 10.1103/PhysRevLett.62.324. URL `https://link.aps.org/doi/10.1103/PhysRevLett.62.324`.

[10] J. E. Hirsch and R. M. Fye. Monte Carlo Method for Magnetic Impurities in Metals. *Phys. Rev. Lett.*, 56:2521–2524, Jun 1986. doi: 10.1103/PhysRevLett.56.2521. URL `https://link.aps.org/doi/10.1103/PhysRevLett.56.2521`.

[11] Philipp Werner, Armin Comanac, Luca de' Medici, Matthias Troyer, and Andrew J. Millis. Continuous-Time Solver for Quantum Impurity Models. *Phys. Rev. Lett.*, 97:076405, Aug 2006. doi: 10.1103/PhysRevLett.97.076405. URL `https://link.aps.org/doi/10.1103/PhysRevLett.97.076405`.

[12] Emanuel Gull, Andrew J. Millis, Alexander I. Lichtenstein, Alexey N. Rubtsov, Matthias Troyer, and Philipp Werner. Continuous-time Monte Carlo methods for quantum impurity models. *Rev. Mod. Phys.*, 83:349–404, May 2011. doi: 10.1103/RevModPhys.83.349. URL `https://link.aps.org/doi/10.1103/RevModPhys.83.349`.

[13] Olivier Parcollet, Michel Ferrero, Thomas Ayral, Hartmut Hafermann, Igor Krivenko, Laura Messio, and Priyanka Seth. TRIQS: A toolbox for research on interacting quantum systems. *Computer Physics Communications*, 196:398–415, 2015. ISSN 0010-4655. doi: 10.1016/j.cpc.2015.04.023. URL `http://www.sciencedirect.com/science/article/pii/S0010465515001666`.

[14] Wei Wu and A.-M. S. Tremblay. Phase diagram and Fermi liquid properties of the extended Hubbard model on the honeycomb lattice. *Phys. Rev. B*, 89:205128, May 2014. doi: 10.1103/PhysRevB.89.205128. URL `https://link.aps.org/doi/10.1103/PhysRevB.89.205128`.

[15] Markus Aichhorn, Hans Gerd Evertz, Wolfgang von der Linden, and Michael Potthoff. Charge ordering in extended Hubbard models: Variational cluster approach. *Physical Review / B*, 70:235107–235107, 2004. ISSN 1098-0121.

[16] Shun-Qing Shen. Topological insulators.

[17] Michel Dyakonov and V I. Perel. Possibility of Orienting Electron Spins with Current. 13:467, 05 1971.

[18] D. C. Tsui, H. L. Stormer, and A. C. Gossard. Two-Dimensional Magnetotransport in the Extreme Quantum Limit. *Phys. Rev. Lett.*, 48:1559–1562, May 1982. doi: 10.1103/PhysRevLett.48.1559. URL `https://link.aps.org/doi/10.1103/PhysRevLett.48.1559`.

[19] Wikipedia contributors. Quantum Hall effect — Wikipedia, The Free Encyclopedia. `https://en.wikipedia.org/w/index.php?title=Quantum_Hall_effect&oldid=848274359`, 2018. [Online; accessed 23-July-2018].

[20] F. D. M. Haldane. Model for a Quantum Hall Effect without Landau Levels: Condensed-Matter Realization of the "Parity Anomaly". *Phys. Rev. Lett.*, 61: 2015–2018, Oct 1988. doi: 10.1103/PhysRevLett.61.2015. URL `https://link.aps.org/doi/10.1103/PhysRevLett.61.2015`.

[21] Cui-Zu Chang, Jinsong Zhang, Xiao Feng, Jie Shen, Zuocheng Zhang, Minghua Guo, Kang Li, Yunbo Ou, Pang Wei, Li-Li Wang, Zhong-Qing Ji, Yang Feng, Shuaihua Ji, Xi Chen, Jinfeng Jia, Xi Dai, Zhong Fang, Shou-Cheng Zhang, Ke He, Yayu Wang, Li Lu, Xu-Cun Ma, and Qi-Kun Xue. Experimental Observation of the Quantum Anomalous Hall Effect in a Magnetic Topological Insulator. *Science*, 340(6129):167–170, 2013. ISSN 0036-8075. doi: 10.1126/science.1234414. URL `http://science.sciencemag.org/content/340/6129/167`.

[22] Chao-Xing Liu, Shou-Cheng Zhang, and Xiao-Liang Qi. The Quantum Anomalous Hall Effect: Theory and Experiment. *Annual Review of Condensed Matter Physics*, 7(1):301–321, 2016. doi: 10.1146/annurev-conmatphys-031115-011417. URL `https://doi.org/10.1146/annurev-conmatphys-031115-011417`.

[23] Christian Griset and Cenke Xu. Phase diagram of the Kane-Mele-Hubbard model. *Phys. Rev. B*, 85:045123, Jan 2012. doi: 10.1103/PhysRevB.85.045123. URL `https://link.aps.org/doi/10.1103/PhysRevB.85.045123`.

[24] M. Hohenadler, Z. Y. Meng, T. C. Lang, S. Wessel, A. Muramatsu, and F. F. Assaad. Quantum phase transitions in the Kane-Mele-Hubbard model. *Phys.*

Rev. B, 85:115132, Mar 2012. doi: 10.1103/PhysRevB.85.115132. URL `https://link.aps.org/doi/10.1103/PhysRevB.85.115132`.

[25] Alexey A. Soluyanov and David Vanderbilt. Computing topological invariants without inversion symmetry. *Phys. Rev. B*, 83:235401, Jun 2011. doi: 10.1103/PhysRevB.83.235401. URL `https://link.aps.org/doi/10.1103/PhysRevB.83.235401`.

[26] Dominik Gresch, Gabriel Autès, Oleg V. Yazyev, Matthias Troyer, David Vanderbilt, B. Andrei Bernevig, and Alexey A. Soluyanov. Z2Pack: Numerical implementation of hybrid Wannier centers for identifying topological materials. *Phys. Rev. B*, 95:075146, Feb 2017. doi: 10.1103/PhysRevB.95.075146. URL `https://link.aps.org/doi/10.1103/PhysRevB.95.075146`.

[27] Stephan Rachel and Karyn Le Hur. Topological insulators and Mott physics from the Hubbard interaction. *Phys. Rev. B*, 82:075106, Aug 2010. doi: 10.1103/PhysRevB.82.075106. URL `https://link.aps.org/doi/10.1103/PhysRevB.82.075106`.